Zehra TAŞ IMAGE PROCESSING BASED MEASUREMENT SYSTEM FOR QUANTIFICATION OF THE TARGET LEUKEMIA CELLS AGU 2019

IMAGE PROCESSING BASED MEASUREMENT SYSTEM FOR QUANTIFICATION OF THE TARGET LEUKEMIA CELLS

A THESIS
SUBMITTED TO THE DEPARTMENT OF ELECTRICAL AND COMPUTER ENGINEERING AND THE GRADUATE SCHOOL OF ENGINEERING AND SCIENCE OF ABDULLAH GUL UNIVERSITY
IN PARTIAL FULFILLMENT OF THE REQUIREMENTS
FOR THE DEGREE OF
MASTER OF SCIENCE

By
Zehra TAŞ
June 2019

IMAGE PROCESSING BASED MEASUREMENT SYSTEM FOR QUANTIFICATION OF THE TARGET LEUKEMIA CELLS

A THESIS
SUBMITTED TO THE DEPARTMENT OF ELECTRICAL AND COMPUTER ENGINEERING AND THE GRADUATE SCHOOL OF ENGINEERING AND SCIENCE OF ABDULLAH GUL UNIVERSITY
IN PARTIAL FULFILLMENT OF THE REQUIREMENTS
FOR THE DEGREE OF
MASTER OF SCIENCE

By
Zehra TAŞ
June 2019

SCIENTIFIC ETHICS COMPLIANCE

I hereby declare that all information in this document has been obtained in accordance with academic rules and ethical conduct. I also declare that, as required by these rules and conduct, I have fully cited and referenced all materials and results that are not original to this work.

Name-Surname: Zehra TAŞ
Signature :

REGULATORY COMPLIANCE

M.Sc. thesis titled Image Processing Based Measurement System for Quantification of the Target Leukemia Cells has been prepared in accordance with the Thesis Writing Guidelines of the Abdullah Gül University, Graduate School of Engineering & Science.

Prepared By

Zehra TAŞ

Advisor

Assoc. Prof. Dr Kutay İÇÖZ

Head of the Electrical and Computer Engineering Program

Prof. Dr. V. Çağrı GÜNGÖR

ACCEPTANCE AND APPROVAL

M.Sc. thesis titled Image Processing Based Measurement System for Quantification of the Target Leukemia Cells and prepared by Zehra TAŞ has been accepted by the jury in the Electrical and Computer Engineering Graduate Program at Abdullah Gül University, Graduate School of Engineering & Science.

…….. /…….. / ……..

(Thesis Defense Exam Date)

JURY:

Advisor: Assoc. Prof. Dr. Kutay İÇÖZ

Member: Prof. Dr. Bülent YILMAZ

Member: Assoc. Prof. Dr. Mustafa TÜRKMEN

APPROVAL:

The acceptance of this M.Sc. thesis has been approved by the decision of the Abdullah Gül University, Graduate School of Engineering & Science, Executive Board dated ….. /….. / …….. and numbered ……..……. .

…….. /…….. / ……..

(Date)

Graduate School Dean

Prof. Dr. İrfan ALAN

ABSTRACT

IMAGE PROCESSING BASED MEASUREMENT SYSTEM FOR QUANTIFICATION OF THE TARGET LEUKEMIA CELLS

Zehra TAŞ

MSc. in Electrical and Computer Engineering Department

Supervisor: Assoc. Prof. Dr. Kutay İÇÖZ

June 2019

Acute Lymphocyte Leukemia (ALL) is the most common type of cancer diagnosed in childhood. The progress of this cancer is quite fast, so time is crucial for the treatment. There are some treatments for patients such as drug therapy (chemotherapy), bone marrow transplantation, radiation treatment, and immunotherapy. Among these treatments chemotherapy is a preferred method, however, its result differs from patient to patient. It is very important to measure the effect of chemotherapy during the treatment in order to adjust the dosage of the drug. Flow cytometry (FC), polymerase chain reaction (PCR) and microscopic examination techniques are used to measure the effect of chemotherapy. However, these methods are time consuming, expensive and require experts. In this thesis, the problem is addressed by an automated cell detection and quantification method based on image processing techniques. The images acquired by optical microscopy were processed and the quantification of ALL cells, which were captured by immunomagnetic beads, was provided. Compared to the conventional methods, this technique is time-efficient, low-cost and easy to use. In addition to the quantification of ALL cells, the image processing algorithms were also developed for the quantification of the magnetic beads that were used in the initial part of the project for signal amplification. The images were acquired from a cell phone microscope for both microscope slide and diffraction grating-based biosensors. In both methods, magnetic bead accumulations were observed. Thus, the accumulation of magnetic beads was detected automatically

Keywords: biosensor, image processing, ALL, magnetic beads, signal amplification

ÖZET

HEDEFLENEN LÖSEMİK HÜCRELERİN SAYIMI İÇİN GÖRÜNTÜ İŞLEME TABANLI ÖLÇÜM SİSTEMİ

Zehra TAŞ

Elektrik ve Bilgisayar Mühendisliği Bölümü Yüksek Lisans

Tez Yöneticisi: Doçent Doktor Kutay İÇÖZ

Haziran 2019

Akut Lenfosit Lösemi (ALL) çocukluk çağında en sık görülen kanser türüdür. Bu kanserin ilerlemesi oldukça hızlıdır, bu yüzden tedavi için zaman çok önemlidir. Hastalar için ilaç tedavisi (kemoterapi), kemik iliği nakli, radyasyon tedavisi ve immünoterapi gibi bazı tedaviler vardır. Bu tedaviler arasında kemoterapi öncelikle tercih edilen bir yöntemdir, ancak sonucu hastadan hastaya farklılık göstermektedir. Hastaların iyileşmesinde ilacın dozajını ayarlamak için kemoterapinin tedaviye etkisini ölçmek çok önemlidir. Kemoterapinin etkisini ölçmek için akım sitometrisi (FC), polimeraz zincir reaksiyonu (PCR) ve mikroskobik inceleme teknikleri kullanılır. Ancak, bu yöntemler zaman alır, pahalıdır ve uzman gerektirir. Bu tezde, sorun görüntü işleme tekniklerine dayanan otomatik bir hücre algılama ve niceleme yöntemi ile ele alınmaktadır. Optik mikroskopi ile elde edilen görüntüler işlenir ve immüno-manyetik boncuklarla yakalanan ALL hücrelerinin ölçümü sağlanır. Geleneksel yöntemlerle karşılaştırıldığında, bu teknik zaman verimli, ucuz ve kullanımı kolaydır. ALL hücrelerinin miktarının yanı sıra, biyosensörlerin sinyal büyütme metodu için projenin ilk bölümünde kullanılan manyetik boncukların belirlenmesi için görüntü işleme algoritmaları da geliştirilmiştir. Görüntüler cep telefonu mikroskopisinden hem mikroskop lamı hem de difraksiyon ızgarası tabanlı biyosensörler için elde edilmiştir. Her iki yöntemde de manyetik boncuk birikimleri gözlenmiş ve geliştirilen algoritmalar cep telefonu mikroskopu görüntülerine uygulanmıştır. Böylece, manyetik boncukların birikimleri bilgisi, görüntü işleme kullanılarak otomatik olarak elde edilmiştir.

Anahtar kelimeler: biyosesör, görüntü işleme, ALL, manyetik boncuklar, sinyal kuvvetlendirme

Acknowledgements

I would like to express my sincere gratitude and appreciation to my advisor Associate Professor Dr. Kutay İÇÖZ. Throughout my masters' degree studies, he has been a great mentor to me. It has been an honor to be his student and a BioMINDS lab member since I was a senior undergraduate student. I would like to thank him for believing me and giving the opportunities to work in his projects.

I also would like to acknowledge my jury members Professor Dr. Bülent YILMAZ and Associate Professor Dr. Mustafa TÜRKMEN, for encouraging me to complete my research and accepting to be members.

I would like to acknowledge THE SCIENTIFIC AND TECHNOLOGICAL RESEARCH COUNCIL OF TURKEY (TÜBİTAK) for supporting my masters' degree studies from the TÜBİTAK projects (Project No: 114E886 and 115E020).

My gratitude also goes to my fellow BioMINDS lab mate Omary MZAVA, who has been working in the same project and has contributed introduction part of this work. He has always been my wise colleague, giving the great advices and supports. My prayers will be always with him. I would also like to acknowledge Rukiye Nur KAÇMAZ, Tayyibe GERÇEK, Albert J. KAHIRA, Esra SÜMER and all AGU graduate students who have played role to complete this work and for making graduate student life perfect.

I also would like to thanks nurse Esma ARSLAN and Dr. Pınar ERDOĞAN for encouraging me to complete my MSc program. I would not complete my thesis without their supports.

Finally, I am grateful to my parents. I always offer thanks for being their daughter. They have been raised me to be auspicious person for humanity, our country and our religion.

Table of Contents

1 INTRODUCTION 1
1.1 AIMS AND CONTRIBUTION OF THESIS 3
1.2 OUTLINE OF THESIS 3

2 BACKGROUND 5
2.1 BIOSENSORS 5
2.1.1 Historical Background of Biosensors 6
2.1.2 Types of Biosensors 7
2.1.3 Application of Biosensors 13
2.2 MAGNETIC BEADS 15
2.2.1 Fundamentals of Magnetism 16
2.2.2 Classification of Magnetic Particles 18
2.2.3 Magnetic Beads Synthesis, Modification and Encapsulation 21
2.2.4 Detection Techniques of Magnetic Particles 23
2.3 SIGNAL AMPLIFICATION METHODS IN BIOSENSORS 26
2.3.1 Nucleic Acid Based Signal Amplification 27
2.3.2 Enzyme Based Signal Amplification 28
2.3.3 1-To-N Binding Based Signal Amplification 28
2.3.4 Magnetic Accumulation Based Signal Amplification 29
2.4 DIFFRACTION GRATINGS 29

3 METHODS 31
3.1 IMAGE PROCESSING BASED DETECTION 31
3.1.1 Binarization 32
3.1.2 Image Filtering (Mean Filter) 33
3.1.3 Morphological Operations 34
3.1.4 Watershed Segmentation 38
3.1.5 Marker-Controlled Watershed Segmentation 39
3.2 CELL PHONE MICROSCOPY 40
3.2.1 Related Works of Cell Phone Microscopy 42
3.2.2 Our Cellphone Microscopy 43

4 RESULTS 47
4.1 MAGNETIC BEADS DETECTION FROM CELL PHONE IMAGES 47
4.2 MAGNETIC BEADS DETECTION ON DIFFRACTION GRATINGS 51
4.3 MAGNETIC BEAD AND CELL DETECTION 55
4.3.1 ALL Cells with CD19s in 100x Magnification Images 56
4.3.2 ALL Cells in 20x Magnification Images 60
4.3.3 ALL Cells Binding CD19 Antibodies in 20x Magnification Images 62

5 CONCLUSIONS AND FUTURE PROSPECTS 68

BIBLIOGRAPHY 70

List of Figures

Figure 1.1 The illustration of bone marrow and blood cells types 1
Figure 2.1.1 The components of biosensors 6
Figure 2.1.2.1 Classification of biosensors…….....8
Figure 2.1.2.1.1 An example of electrochemical biosensor called i-STAT. The device can analyze blood samples in a few minutes…….9
Figure 2.2.1.1 Hysteresis curve. 18
Figure 2.2.2.1.1 Magnetic moment alignment for ferromagnetic materials. 19
Figure 2.2.2.2.1 Magnetic moment alignment for antiferromagnetic materials. 20
Figure 2.2.2.4.1 A non-hysteretic M-H curve of superparamagnetic materials 21
Figure 2.4.1 Diffraction gratings for detecting of S-adenosyl homocysteine using SAH-Ab beads. Scale bar is 30μm 30
Figure 3.1.1.1 It is an example of the local thresholding sets the threshold value by combining the local thresholding around objects 33
Figure 3.1.3.1.1 The images illustrates some of the example of morphological structuring elements and the shaded pixels represent the center pixel of structuring elements 34
Figure 3.1.3.1.2 The local neighborhood determined by the structuring element. This is defined by those shaded pixels in the image, which lie under the pixel value having 1 in the structuring element 35
Figure 3.1.3.2.1 It is an example of a dilated image. The left image is a sample image; the right image is the dilated image with represented structuring element below of images 36
Figure 3.1.3.3.1 Illustration of the effect of opening and closing operations over some example shapes. The images to the left represent the opened original image placed in the center with the structuring element has radii 3, 5, 15 top to bottom. The images to the right represent the closed original image with structuring element has radii 3, 5, 25 top to bottom 37
Figure 3.1.4.1 Watershed algorithm flooding simulation 38
Figure 3.1.5.1 Direct application of watershed on gradient images often resulting in over segmentations 39
Figure 3.1.5.2 Marker controlled watershed segmentation given in Matlab Image Processing Toolbox 40

Figure 3.2.1 The illustration of microscopes (A) It is an example of an optical microscope [125] . (B) It is an example of a new generation mobile phone which can be turned into cell phone microscopy 41
Figure 3.2.1.1 (A) A cell phone microscopy capable of both fluorescence and bright field images created by [125]; (B) The system is created with a microscopic platform and it is called compact and lightweight microscope [136]; (C) a mobile phone microscopy that uses spherical ball lens as a microscope lenses for the point-of-care diagnosis of soil-transmitted helminths 43
Figure 3.2.2.1 The illustration of the images recorded in the same area from optical microscopy and cell phone microscopy, respectively. (A) The image is taken from Nikon SE with 40x magnification. (B) The image is taken from cell phone microscopy using Samsung Note 4 with spherical ball lens having 100x magnification. 44
Figure 3.2.2.2 Cell phone microscope with a spherical ball lens. (A)Illustrates the crucial parameters of spherical ball lens; (B) The cell phone microscopy setup; (C) The measurement setup schematic. 45
Figure 4.1.1 Cell phone microscopy based on image processing with cloud server. 48
Figure 4.1.2 The image processing method applied to cell phone microscopy images. (a) RGB image used as an input; (b) grayscale image converted from RGB; (c) binary image, obtained using mean and standard deviation method; (d) filtered binary image using morphological operations: imclearborder and bwareaopen; (e) the boundaries of magnetic beads chain and numbers on plotted on original image by filtering background noise to user for the selection of desired chain information; (f) selected chain information, for this example second chain was selected.. 50
Figure 4.2.1 Images of self-assembled gratings by varying concentrations of immunomagnetic beads on micro-contact printing acquired by cell phone microscope and optical microscope used as a reference microscope. The top row is recorded from the optical microscope (Nikon) and the second row is recorded from the cell phone microscope. The bottom row is processed images acquired by the cell phone microscope.. 52
Figure 4.2.2 An example of the result of the image processing method applied to images taken from 0.67 mg/mL solution. (A) original image; (B) gray scale image; (C);

background subtracted image; (D) adjusted image; (E) boundaries of magnetic beads plotted on the original image.. 54
Figure 4.3.1 Illustration of data acquisition for image processing procedure. 55
Figure 4.3.1.1 The flowchart of image processing for 100x magnification images. 57
Figure 4.3.1.2 The explanation of the image-processing algorithm. (A) The original image taken from microscope the arrows show the ALL cells and CD19 antibodies; (B) The grayscale image transformed from original image;(C) The binary image converted from the grayscale image using Otsu's multithresholding method;(D) The regional minimums obtained from application of distance transform algorithm and regional minimum functions (E) Applied watershed transform algorithm on (D); (F) Plotting the number of beads segmented via watershed; (G) The first approach of eroding beads using regional properties to create a mask; (H) The second approach of eroding beads applying erosion and dilation on binary image to create a mask. The scale bar is 20 μm for each image. 59
Figure 4.3.2.1 The flowchart of quantification of ALL cells in 20x magnification images. 60
Figure 4.3.2.2 (A) is an original image taken in RGB; (B) is the grayscale image converted from RGB image; (C) is the opened image after applied average filter to grayscale image shown in B; (D) is the modified image using background subtraction method obtained by subtraction opened image (D) from the grayscale (B). The scale bar is 20 μm for each image. 61
Figure 4.3.2.3 (A) represents the adjusted image obtained by adjustment and dilation; (B) illustrates the regional maxima obtained by A; (C) is the reconstructed image represents the ALL cells; (D) the final image of quantification of ALL cells without CD19 antibodies. 62
Figure 4.3.3.1 The flowchart of image processing algorithm for the quantification of ALL cells binding CD19 antibodies in 20x magnification images taken from the optical microscope. 63
Figure 4.3.3.2 (A) is the original image; (B) is the binary image; (C) illustrates regional minima in the binary image that it is obtained to apply watershed; (D) illustrates the CD19 beads quantification that the segmented beads plotted on the original image; (E) and (F) are cropped images from D to show segmentation better. The scale bar is 20 μm for each image..... 65

Figure 4.3.3.3(A) is the original image; (B) is the obtained image after eroding the magnetic beads from original image; (C) The application of background subtraction on B; (D) illustrates the regional maxima after adjusting C and finding maximum field in the image; (E) illustrates the reconstructed images obtained by morphological operations that are used to label the blobs and quantify them; (F) shows the detected ALL cells in the image; (G) and (H) is the part of the resulting image zoomed to show the ALL cells clearly. The scale bar is 20 μm for each image. 67

List of Tables

Table 3.2.2.1 Parameters of spherical ball lens (all distance are in units of μm). 45

To my lovely country

I will always do my best

Chapter 1

1 Introduction

Blood is an indispensable material for the survival of human. It is produced in bone marrow, which is a spongy structure inside the bone. Blood cells in the bone marrow are produced initially as stem cells then developed into three types of blood cells that are Red Blood Cells (RBCs), platelets and White Blood Cells (WBCs). The illustration of bone marrow and blood cell types are shown in Figure 1.1.

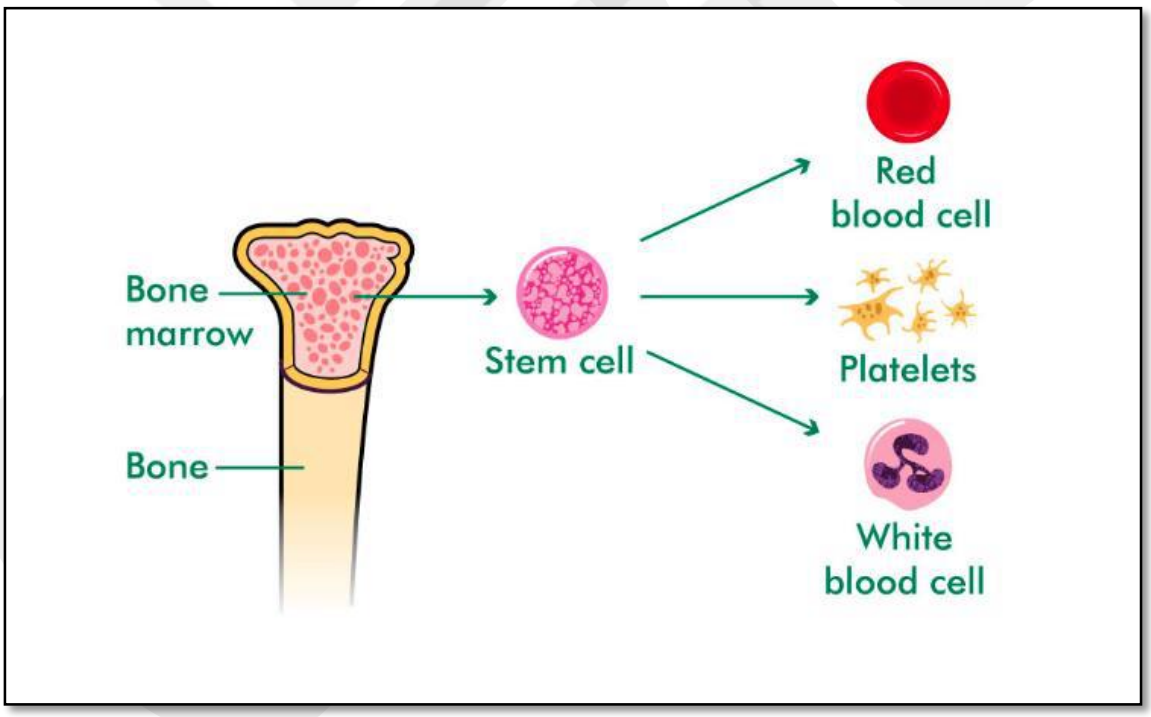

Figure 1.1 The illustration of bone marrow and blood cells types [1].

RBCs are responsible of carrying oxygen from the lungs to all cells in the body and carbon dioxide from all cells to the lungs. Platelets are responsible of plugging up the holes in the blood vessels caused by injury. WBCs are protection cells in the body

that fight against infections and they have three main types lymphocytes, granulocytes, and monocytes.

Acute Lymphoblastic Leukemia (ALL) is a disorder occurs when lymphocytes grow abnormally in WBCs and it quickly affects the patient. ALL is the most common cancer type in childhood, according to American Cancer Society [2]. The early diagnosis of ALL is crucial for treatment of patients. However, ALL can relapse after recovery that is called Minimal Residual Disease (MRD). In general, children with MRD during or after the chemotherapy are more prone to have relapses thus, they need more intense treatment [3]. There are several diagnosis methods for MRD such as flow cytometry [4], polymerase chain reaction and microscopic exams [5]. However, flow cytometry and PCR are expensive techniques and they require long processing time. In microscopic exams, an expert counts blood cells under a microscope. Although this method is efficient, manual counting is time consuming and not efficient, and it is lack of standard accuracy because of depending on personal skills [6].

In this thesis, we focus on developing an automated image processing system for quantification of ALL cells, which is not manual, cheaper than flow cytometry and PCR, and does not need much time.

In literature, there have been many researches based on automated image processing methods for counting, detecting and quantifying of cells that we reviewed to develop our approach.

Automated counting and diagnosing of malaria in microscopic images [7]–[9] are reported based on image processing and computer vision. Segmentation of overlapping objects [10], segmentation and classification of magnetic particles [11] are effective examples for segmentation process. There are also segmentation researches for red blood cells [12] in digital holographic microscopy, white blood cells segmentation based on cell color and shape [13], cell nuclei segmentations [14] based on watershed transformation and [15], [16] based on marker controlled watershed and cell nuclei segmentation in fluorescence microscopy images [17], segmentation of clustered cells [18] in negative phase contrast images that are reported. Moreover, the fish disease diagnosis [19], cell quantification on HIV microfluidic devices [20], automated cell counting [21] have been provided based on microscopic image processing. Furthermore, automated leukemia detection [22], [23], automated leukemia cell counting [6], [24], segmentation of leukocytes [25] and leucocyte classification [26] have been reported for analyzing cancer disease based on image processing for microscopic images.

1.1 Aims and Contribution of Thesis

This thesis is built on two main image-processing algorithms for optical microscope images and cell phone microscope images. The optical microscopy images were acquired for quantification of ALL cells and the cell phone microscopy images were taken for quantification of magnetic beads smeared on a microscope slide and located on micro-contact printed lines.

As explained above, ALL is a type of cancer, which required quick diagnosis and treatment for the recovery of patients. Despite other diagnosis methods, we worked on an automated quantification system based on MATLAB Image Processing Toolbox. The provided automated system is cheap, easy to use and fast. In order to capture target ALL cells, the immunomagnetic beads were prepared and used to bind to target cells. The mixture of ALL cells and immunomagnetic beads solution was smeared on the microscope slide and the images were acquired by using an optical microscope. The image-processing algorithm was employed on the image and the magnetic beads and ALL cells were counted and the meaningful information of them was gathered.

In addition to quantification using the microscopic images, image-processing algorithms were developed for cell phone images to quantify magnetic beads. Firstly, cell phone images were recorded from the microscope slide to detect magnetic accumulation-based signal amplification as explained in 2.3.4. This study opened up a new signal amplification method using magnetic beads and point of care testing using a cell phone. Secondly, cell phone images were recorded from micro-contact printed lines. For this study, the aim was to prove that the quantification of binding magnetic beads on the surface of printed lines is possible with the cell phone microscopy.

1.2 Outline of Thesis

In this thesis, there are four chapters to give aim, background information, methods, results and conclusion.

In Chapter 2, the brief explanation of biosensors, magnetic beads, signal amplification from magnetic beads and diffraction grating will be introduced. The

background information of this thesis will be explained to understand the fundamentals of the image processing, diffraction gratings and ALL cells.

In Chapter 3, the image processing methods that we used for our work will be explained. Then, the cell phone microscopy method together with the cell phone microscopy set-up will be explained.

In Chapter 4, firstly, image-processing results will be explained for magnetic bead detection using cell phone images. Secondly, the results of the algorithm for cell phone images taken for the diffraction gratings will be clarified. Finally, the results of the image-processing algorithm will be explained for the quantification of ALL cells and immunomagnetic beads for the images acquired from the optical microscope.

In Chapter 5, the conclusion of the thesis and future prospects will be explained.

Chapter 2

2 Background

This chapter is devoted to explain the background information of the topics this thesis constructed upon. Firstly, the biosensors, characteristics of a biosensor, history, components and its categories along with applications of them will be explained. Secondly, the magnetic particles/beads, their characteristics, detection types in biosensors will be introduced. Thirdly, the signal amplification methods in biosensors will be explained with sub-section magnetic accumulation based signal amplification. Finally, a brief explanation of diffraction gratings will be given.

2.1 Biosensors

A biosensor is an analytical device that captures a biological response and converts it into an electrical signal that proportional to the concentration of the analyte in the reaction [27]–[29]. An analyte is a material of interest that needs detection. This material of interest could be bacteria, viruses, nucleic acid, protein, and cell. For instance, glucose in human blood is an analyte in a biosensor design for detection of glucose level.

A biosensor has three main components: a bioreceptor/biomolecular probe, transducer and signal processor as shown in Figure 2.1.1.

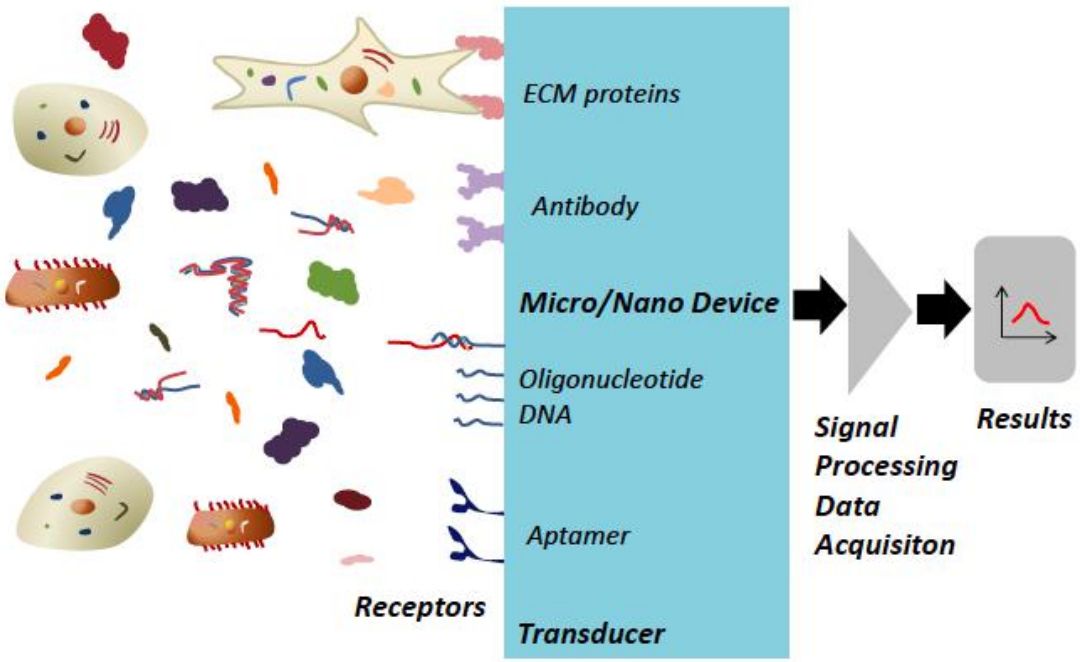

Figure 2.1.1 The components of biosensors [30].

The bioreceptor/probe is an immobilized biological element that specifically recognizes the target analyte in the sample. The probe may be proteins, enzymes, aptamers, cells, deoxyribonucleic acid (DNA) and antibodies, which interact with the desired analyte and produce biological signals that proportional to the concentration of the target analyte.

The transducer is a detector element that transforms the biological signal resulting from the interaction between probe and analyte into measurable signals. The measurable signals could be an optical, electrical, electrochemical, mechanical, acoustic, magnetic or could be a combination of signals based on system design [31]. The last part of the biosensors is the signal processing unit which process transformed signal via necessary electronics, amplifiers, and filters and display it in a user-friendly way [32].

2.1.1 Historical Background of Biosensors

Although, the history of biosensor dates back to the early 1900s, the first true biosensor was demonstrated for oxygen detection by Professor Leland C. Clark, in 1956 [33]. He is known as ‘Father of Biosensors’ and the name is given to his invention of oxygen electrode: ‘Clark Electrode’ [34]. Later on, Leland C. Clark expanded the design and construction of electrode systems and related electronic instrumentation for

measuring of glucose level in blood [35] and he coined the term “enzyme electrode” in this paper [33]. Thus, he opened up the measurement of blood ions, sugar, and urea utilizing the developments of biosensor technology. Then subsequently in 1967 Updike and Hicks used the same term “enzyme electrode” for a similar device in which the enzyme glucose oxidase was immobilized in a polyacrylamide gel onto a surface of an oxygen electrode for the rapid and numerical analysis of glucose [36]. Besides amperometry, the first potentiometric biosensor was discovered to detect urea in 1969 by Guilbault and Montalvo, Jr [37]. Eventually, the first commercial biosensor was designed for measuring the glucose level in human blood in 1975, by Yellow Spring Instruments [38].

Since then, significant progress has advanced in the field of biosensor technology. Today, the field is a multidisciplinary area of research that assembles various sciences such as physics, chemistry and biology and material science with fundamentals of micro/nano-technology, electronics, and applicatory medicine. According to Science Direct database, over 25,000 research papers have been published in three years (2016-2019).

2.1.2 Types of Biosensors

Biosensors can be grouped into two major classes: based on their biorecognition elements and transduction mechanism. These classes together with subclasses are explained in Figure 2.1.2.1 and a brief explanation of some of them is given below.

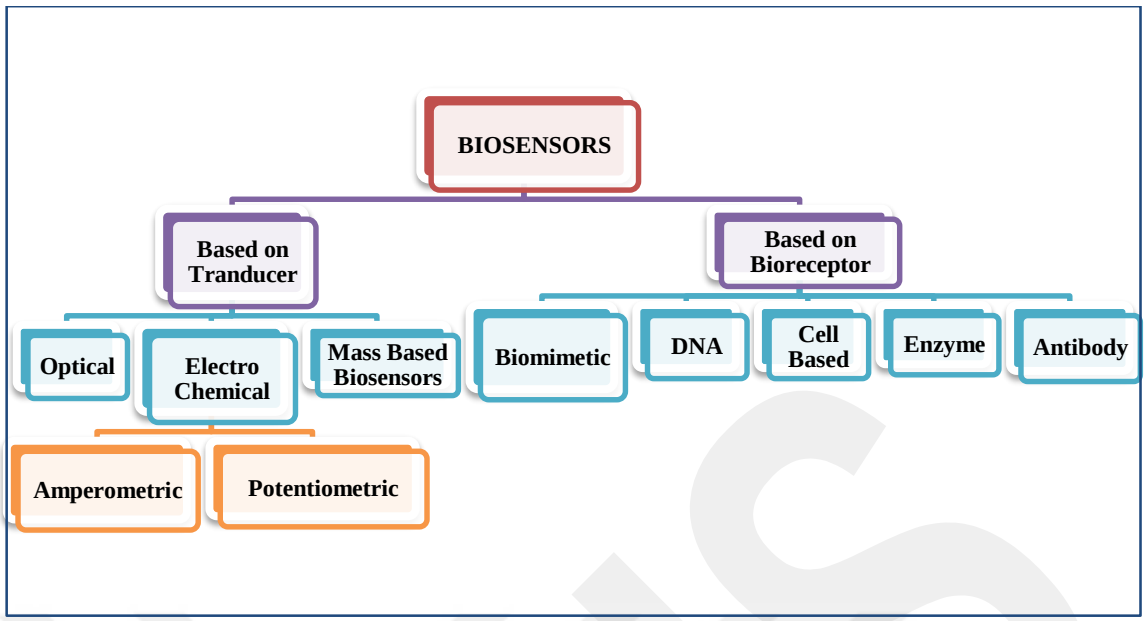

Figure 2.1.2.1 Classification of biosensors.

2.1.2.1 Based On Transduction Mechanism

Transduction can be achieved through an enormous variety of methods. Most forms of transduction can be group into three main categories. These are 1) electrochemical detection methods, 2) optical detection methods and 3) mass detection methods. Despite these three main categories, the new types of transducer have been advanced in biosensors lately. Each of these three main groups involves a lot of subgroups, produced an almost infinite number of transduction methods or/and combinations of methods.

Electrochemical Biosensors

The first biosensor that is based on the electrochemical transduction method published along with successfully commercialized was represented in [35]. In this work, only the detection of glucose oxidase (GOx) was defined. Although glucose oxidase is still the most common analyte, progression in the biosensor technology enable to detect multiple analytes [32], [39], [40]. Today, there are many works based on this approach and most of them already commercialized such as [41], [42]. In these studies, the biosensor called i-STAT has easy to use interface. This device provides users a comprehensive bedside testing platform, which tests cardiac markers, lactate chemistries, blood gases, coagulation and hematology in a few minutes. The image is

shown in Figure 2.1.2.1.1 An example of electrochemical biosensor called i-STAT [42]. The device can analyze blood samples in a few minutes.

Figure 2.1.2.1.1 An example of electrochemical biosensor called i-STAT [42]**. The device can analyze blood samples in a few minutes.**

The principle of the electrochemical biosensor is that the immobilized biomolecular probe binds the target analyte to generate a chemical reaction by producing or consuming ions or electrons. The production and consumption of electrons or ions affect the measurement of the electrical characteristic of the solution, such as current, potential [39], [43]. These approaches use the amperometry, potentiometry and voltammetry techniques, which are subcategories in accordance with measured signals.

An amperometric biosensor is based on measurement of the current resulting from the oxidation or reduction of an electroactive analyte species under constant potential. The resulting current magnitude is directly correlated to the concentration of the analyte [44]. The conventional example of an amperometric device is the aforementioned glucose biosensor which detects hydrogen peroxide based on amperometry [38].

Potentiometric biosensors measure the potential difference in the working electrode compared to the reference electrode, or two reference electrodes separated by term selective membrane, when there is no current flow between them [45], [46]. The most known potentiometric biosensors are pH electrodes. The potential differences between the reference electrode and the working electrode are proportional to the logarithm of the ion activity or concentration. Thus, they give information about ion activity and this makes them very useful in bioavailability or speciation studies [47].

Optical Biosensors

Optical biosensors are pretty sensitive devices that principally gather measurable signals from an analyte by using photons [48]. They are the most distinctive types of biosensors because of their different types of spectroscopy. For instance, absorption, refraction, fluorescence, diffraction, Raman, scattering, phosphorescence and Surface Enhanced Raman Spectroscopy (SERS) are spectroscopic methods used in optical biosensors. Among these properties, the amplitude is the most common measurement component because it is directly connected with the concentration of the desired analyte [49]. In optical biosensors, there are optical fibers that allow detecting the target analyte using absorption, fluorescence, transmitting and scattering of light [50]. In general, the signal obtaining from an optical biosensor is provided by optical fibers/flexible cables, which transmit light to a biological constituent. There are a lot of methods that have been utilized in these types of biosensors. Among all surface plasmon resonance, fluorescence spectroscopy, interferometry, and spectroscopy-based devices are the most common types.

Mass Based Biosensors

Mass sensitive biosensors are based on resonation of piezoelectric quartz crystal in a fundamental frequency. The basis technic of this biosensor is that the piezoelectric crystal functionalized by a biomolecular probe such as an antibody, enzyme, etc. so this compound becomes highly susceptible to target analyte. When the compound subject to the desired analyte, the absorption occurs that causes a frequency variation, which is employed to measure the amount of absorption. These biosensors are the most common type among transducer based biosensors [51]. In application, they have a great property for the detection of pathogens [52].

2.1.2.2 Based on Bioreceptor

A bioreceptor/ biomolecular probe is a significant part of a biosensor because of its role in recognition of the desired analyte into the biological sample. A biomolecular probe has a high binding affinity to an analyte as much as stability. Thus, the selection of bioreceptor depends on both the target analyte and the characteristic of receptors.

Enzyme Based Biosensors

Biosensors based on enzyme as recognition elements perform one of the most prevalent studies. In enzymatic biosensors, the enzyme is used as a bioreceptor, which specifically recognizes substrates and catalyzes their transformation. These unique abilities make them important tools in biosensor technology [53]. The working principle of them based on that the product of response catalyzed by enzymes can be determined either directly or along with an indicator [54]. Enzyme-based biosensor provides to explore much lower limits than normal binding techniques. Glucose oxidase (GOD) and horseradish peroxidase (HRP) is the most commonly used of enzymatic biosensors, however, these biosensors also can be employed to detect cholesterol, environmental monitoring, food safety, heavy metals and also pesticides [55].

Immunosensors

The first antibody-based biosensor was introduced in the 1950s and it paved the way for immuno-diagnosis [53]. Since then, there have been numerous studies to develop immunosensors, which include an antibody as a bioreceptor for clinical diagnostics. Antibodies, also known as immunoglobulins, utilize the ability to bind with the corresponding antigens, which is highly specific and diverse, they can also be immobilized on biosensor component or surface. Antibodies can significantly improve the detection boundary and productivity of a biosensor because of their powerful binding constant and high specificity [5],[30]. These specifications provide immunosensors to be employed in wide areas such as clinical diagnosis, food quality and environmental monitoring [57]. The improvements of immunosensors for bacteria and pathogen detection has gained a significant role due to their applications in the point of care measurements (POC) [58]. Furthermore, immunosensors have been used

for imaging of tumors or visualizing tumor shrinkage or circulating tumor cell detection [53], [55], [59].

DNA/Nucleic Acid Sensor

The nucleic acid-based biosensors use the complementary relationship between adenosine and thymine and cytosine and guanosine in DNA form the basis of affinity binding specificity. Two single-stranded DNA (ssDNA) chains to form one double-stranded DNA (dsDNA) are employed for these types of biosensors. The working principle based on that an immobilized base ssDNA is used to detect the complementary of ssDNA to form dsDNA. These biosensors have a significant role in the detection of viruses and diseases in clinical diagnostics and biomedical applications [60].

Cell-based biosensors

Cell-based sensors are special types of biosensors, which use immobilized living cells as a bioreceptor combined with transducers to detect the intracellular and extracellular microenvironmental condition, physiological parameters, and composes a response using the interaction between cell and stimulus [61]. Living cells such as bacteria, fungi, yeast, algae, proteins that are present in cells, and tissue-culture cells (from animals or plants), can be employed as a bioreceptor to detect the target of the sample [57], [62]. The living cell-based biosensor is a unique type compared to other types of biosensors that have materials extracted from living stuff. The recent researches represent that cell-based biosensors have become a rising device for different research areas like medical diagnosis [63].

Biomimetic biosensors

A biomimetic sensor is an artificial or a synthetic biosensor that works based on mimicking the natural sensors. An aptasensor is an example of a biomimetic sensor, which uses an aptamer as a bio component. Aptamers are the synthetic short oligonucleotides (RNA or ssDNA) that can be employed to detect amino acids, oligosaccharides, peptides, and proteins [55]. These types of biosensors have a wide range of areas include clinical diagnostic to recognize pathogen, virus and infectious diseases [64]–[66].

2.1.3 Application of Biosensors

Biosensors have been commonly used in numerous scientific disciplines via their outstanding results [29]. They have many advantages compared to other analytical devices due to their selectivity, sensitivity, and specificity. Moreover, they are low cost, small size, easy to use and rapid. Developments in biosensor technology provide many biosensors to been commercialized for recognizing biomolecules onsite. The emerging technologies in lab-on-a-chip and micro/nano biosensors also offer changes to create new biosensors with much better productivity [67]. Biosensors have been depicted to play an important analytical role in various fields such as medicine, agriculture, food safety, homeland security, bioprocessing, environmental and industrial monitoring [68]. The introduction of application and some examples about them are given in the following section.

2.1.3.1 Clinical and Diagnostic Application

Among the various application area of biosensors, medical diagnostics and monitoring are the most important fields. Nowadays, there are huge numbers of people affected with varied diseases such as diabetes, obesity, heart diseases and cancer [69] that these diseases need medical care. The diagnosis and monitoring of diseases involve a lot of effort for a routine blood sample and other related tests. Conventional techniques need specialized person, a long time and high sample volumes. However, biosensors have much more advantages than conventional techniques since their size, selectivity, low cost, high sensitivity and easy operation for the target analyte. Also, they don’t need a specialized person and expensive instrumentation that enable them for home care diagnostics.

Glucose biosensor is one of the most commonly used biosensor types. According to WHO report, about 422 billion people in the world have diabetes [70]. The self-monitoring of glucose level in blood is crucial for the prognosis of diabetes. he glucose biosensor allows the patient self-testing in the clinic, at home in the workplace where it is needed [32], [51], [67].

The other commonly used biosensor is human chorionic gonadotropin (hCG) biosensor known as a pregnancy test. It is the most successful home-use-protein detection biosensor which detects hCG in urine [71].

Biosensors have been also utilized in the detection of cancer and cardiac biomarkers, different hormones, virus, cancer cells as explained in [55], [68], [72], [73].

2.1.3.2 Food Analysis

Food quality and safety are important tools for human health. Biosensors have been used to analyze food quality, security (detection of compound contaminants, allergens, toxins, pathogens, additives, etc.) and online process control. Moreover, biosensors are used for other significant analytes such as sugars, alcohols, amino acids and flavor. Biosensors provide a confidential analytical result for quality control and production process of foods due to their specificity, sensitivity and velocity. As an example, commercially available biosensors are given for food analysis in [67].

2.1.3.3 Environmental Analysis

Growing global economy and industry bring with employing chemical compounds in agriculture, which endanger to release many toxic mixtures into water, soil and air. Synthetic chemicals, pesticides, and heavy metals are the main contamination of environmental pollution, which can enable the disease to humans and animals. The diagnosis and monitoring of toxic chemicals are crucial for the safety and security of human being and overall environment, as well. Biosensors are very important devices for environmental analysis such as the assessment of contaminated water [74].

2.1.3.4 Biodefense

Over the past two decades, different viral, bacterial agents and toxins are used as biological warfare agents by terrorists that have been become an important threat. Biosensors can be used for the detection and quantification of chemical and biological warfare agents (BWA) in real-time monitoring. Rapid and sensitive detection of BWA is crucial for both early diagnosis and successful treatment after exposure of BWA. To achieve this, some research working on biodefense biosensors such as [75].

2.2 Magnetic Beads

Micro/Nanoscience is one of the most crucial research areas in modern science. Nanotechnology opens up new detection techniques in the molecular and cellular levels to a researcher in biomedical, biotechnology, engineering, environmental and material science [76], [77]. Using magnetic beads in nanotechnology offers various advantages due to their physical and chemical properties. Some of them are:

First, they can be produced/synthesized at a selective size ranging from micrometer to nanometer scale. The application where they are used, the size flexibility is a crucial factor. This feature ensures that the size of the magnetic beads is close to the size of the biological entities such as cell (10-100μm), virus (20–450 nm), a protein (5–50 nm) or a gene (2 nm wide and 10–100nm long). Additionally, magnetic beads can be coated with different coatings e.g. polymer, which makes them bind or interact with the target biological entity. This interaction offers to label target biomolecules or to address them.

Second, magnetic beads are magnetic, which means that they can be guided or manipulated by an external magnetic field gradient, so no residual magnetism left in the absence of a magnetic field. Using a controlled magnetic field provides a mechanism for remotely measuring and regulating the biological environment, so this property opens up doors for in vitro and in vivo biomedical applications.

Third, magnetic nanoparticles can be made to respond to an applied external magnetic field that is time-varying. This causes energy to be transferred from the magnetic field to the nanoparticles, which paves the way for many applications [78].

Fourth, they can be detected via several methods as a result of their unique properties.

Generally, designing magnetic particles (MPs) for a specific application have some process, including: synthesizing MPs with a proper size, modifying them with a proper biocompatible linker and suitable ligands, making suitable size of them and ligand to optimize magnetic properties for a specific application and selecting the optimal detection technique for testing and using MPs [79].

Current studies make available different types of magnetic particles in today. Among them, iron oxides and especially magnetite (Fe_3O_4) and its oxidized form maghemite (γ-Fe_2O_3) have captivated much attention due to their biocompatibility, low

toxicity, and easy preparation at low cost [80]. Cobalt and Manganese oxides have more attractive properties, however, their high toxicity oxidative sensitivity makes them less favorable [81].

Magnetic particles' property, surface chemistry and types of magnetic particles are important features for a suitable application where they are used.

2.2.1 Fundamentals of Magnetism

In principle, a magnetic field is produced by the movement of the free electric current inside the material or by magnetic materials, like permanent magnets [82]. When the free (externally controllable) electric current moving through a conductor, the magnetic field strength $\boldsymbol{H}$ can be measured, whose SI unit is Ampere-Turns per unit meter (A/m). When a material is steered by an external magnetic field, the individual atomic moments contribute to the entire response of that material to the field [78], [83]. This response is defined as magnetic induction or magnetic flux density represented by $\boldsymbol{B}$ is measured in Tesla (T) or weber/m^2 in SI units.

When an external magnetic field applied to a material, the response of the material is named as the magnetic permeability of the material **(μ).** In free space, the relationship between the material and the magnetic field is linear, so we have the permeability of free space $\boldsymbol{\mu_0}$**.** However, in most cases, the relationship is not linear in any other medium. But, μ can be varied with the applied magnetic field.

$$\boldsymbol{\mu_0 = \frac{B}{H}} \qquad \textbf{(2.2.1.1)}$$

$$\boldsymbol{B = \mu H} \qquad \textbf{(2.2.1.2)}$$

Magnetic fields produced by magnetic materials are the consequences of a magnetic moment per volume, which is the so-called magnetization $\boldsymbol{M}$ inside the material. It is obtained by the following equation,

$$\boldsymbol{M = \frac{m}{V}} \qquad \textbf{(2.2.1.3)}$$

$\boldsymbol{m}$ is the magnetic moment; $\boldsymbol{V}$ is the volume of the material.
Under an applied magnetic field, the final relationship;

$$\boldsymbol{B = \mu_0(H + M)} \qquad \textbf{(2.2.1.4)}$$

this equation is straight for all magnetic systems.

All materials display magnetic properties according to their atomic structure and temperature. Under certain cases, some of them display strong magnetism, such as iron, cobalt and nickel, while others display weak magnetism (paramagnetic) or are slightly antimagnetic (diamagnetic). This event is best clarified by magnetic susceptibility χ, given by the following equation;

$$\boldsymbol{\chi = \frac{M}{H}} \qquad \textbf{(2.2.1.5)}$$

Here χ is a volume dimensionless phenomenon that it is the sign of the classification of materials behavior under applied magnetic field. If the materials have small magnetic susceptibility, then that they are less magnetic and vice versa.

In materials, all electrons are paired in atomic or molecular orbitals by spinning up and spinning down, and all spins cancel each other therefore no net magnetization can be induced. However, unpaired electrons do not have this limitation, so they contribute to the net magnetization of the material. Without an external magnetic field, the unpaired spins move randomly, thus they cancel each other on a microscopic level and the total magnetization is zero. When an external magnetic field is applied, the unpaired spins start to line up, thereby they conduce a net magnetization. This alignment deals with temperature, which is inclined to randomize spin orientation. At low temperatures, aligning all the spins is possible at the high magnetic field and

saturates the magnetization. However, when the temperature rises, the strength of the magnetic field decreases [82].

Figure 2.2.1.1 is the hysteresis loop shows the magnetic properties of magnetic materials including ferromagnets. The applied magnetic field illustrates magnetic fields $\mu_0 \boldsymbol{H}$ on the x-axis and the total magnetic field $\boldsymbol{B}$ or $\boldsymbol{M}$ on the y-axis. For ferromagnetic particles $\boldsymbol{B}$ is given by predominantly $\boldsymbol{M}$, because $\boldsymbol{H}$ is negligible compared to $\boldsymbol{M}$**.** When the external magnetic field applied, the magnetic moment of the material is aligned along with the external field direction. The maximum magnetization is represented as the saturation magnetization M_s. When the external magnetic field is reduced to zero, the magnetization of these materials is prone to retain the previous magnetization, which is called the remnant magnetization M_r. In order to bring net magnetization zero, an applied magnetic field is necessary for the opposite direction.

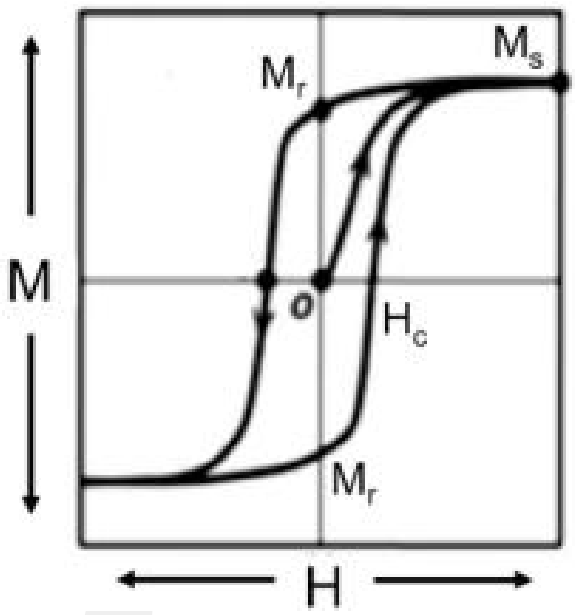

Figure 2.2.1.1 Hysteresis curve.

2.2.2 Classification of Magnetic Particles

Magnetic particles are classified in different types of groups based on their atomic structure and their magnetic response. The types are ferromagnetic beads, antiferromagnetic beads, ferrimagnetic beads, paramagnetic beads and superparamagnetic beads.

2.2.2.1 Ferromagnetism

Ferromagnetic materials display magnetism even the absence of an applied external magnetic field. Accordingly, ferromagnetism is responsible for permanent magnetism. The unpaired electrons in materials have positive exchange energy and a significant mutual interaction, they align parallel to each other in the region called domain, shown in Figure 2.2.2.1.1. There is an important imbalance in the domains; therefore there is no net magnetization because of randomly aligned domains. Upon the applied magnetic field, the domains tend to align in the same direction with the magnetic field and the net magnetization experienced.

They try to keep their magnetization after the removal of the external magnetic field, so their magnetism does not return to zero. This property is used in the fabrication of permanent magnets.

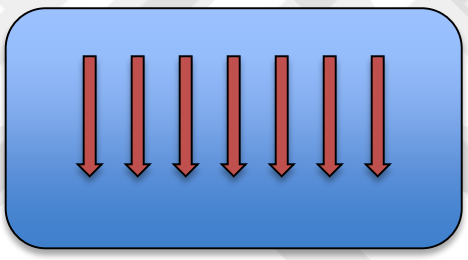

Figure 2.2.2.1.1 Magnetic moment alignment for ferromagnetic materials.

2.2.2.2 Antiferromagnetism

The magnetic property of antiferromagnetism is similar to ferromagnetism. The difference between them is that the unpaired electrons in antiferromagnetic materials are anti-parallel in Figure 2.2.2.2.1. Thus, the overall net magnetization is zero. The susceptibility of them is small and positive. Antiferromagnetism becomes destroyed by thermal agitation, which is called as Neel temperature. Above this temperature, antiferromagnetic materials act as paramagnetic materials.

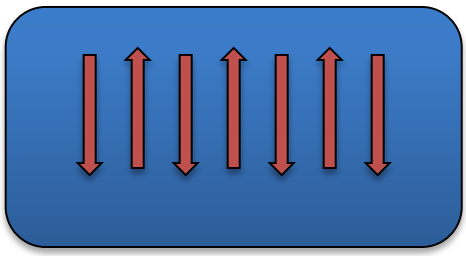

Figure 2.2.2.2.1 Magnetic moment alignment for antiferromagnetic materials.

2.2.2.3 Paramagnetism

Without an external magnetic field, the electrons in the domain of paramagnetic material equally populated with spin-up and spin-down. When an external magnetic field is applied, the electrons tend to move through unfilled domains, thus the weak magnetization is observed. Paramagnetic materials have small magnetic susceptibility the order of 10^{-6} to 10^{-1}. When the external magnetic field is removed, they immediately lose their magnetism [83].

2.2.2.4 Superparamagnetism

Superparamagnetism consists of very small single domain ferromagnets or ferrimagnets. In this situation, the thermal energy can transform the direction of the magnetization. Therefore, the average magnetization becomes zero and the material behaves sort of paramagnet. However, the material has small a single domain and the susceptibility of the material bigger than the paramagnetic, hence it is classified as superparamagnetic. In the absence of an applied magnetic field, they have negligible remnant magnetization. When an external magnetic field is increased, the magnetization of superparamagnetics increase like paramagnetics [79] .

The property of superparamagnetism is shown in Figure 2.2.2.4.1.

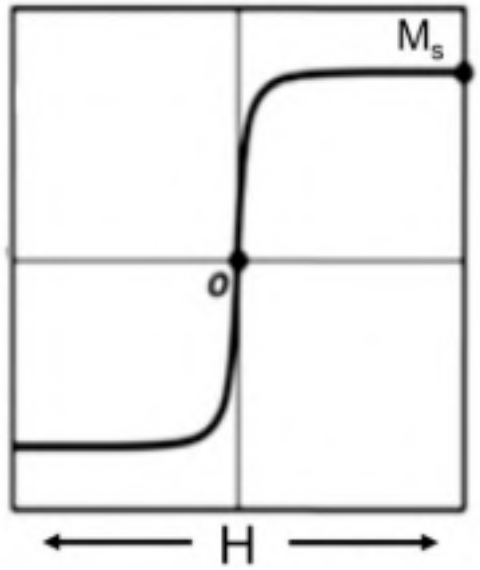

Figure 2.2.2.4.1 A non-hysteretic M-H curve of superparamagnetic materials [79]**.**

2.2.3 Magnetic Beads Synthesis, Modification and Encapsulation

Several approaches about fabrication and synthesis techniques of magnetic nanoparticles have been studied and some reviews available in [84]–[86]. Despite pure metals have desired magnetic properties, their high toxicity and oxidative sensitivity make them unsuitable for biomedical applications without appropriate treatment [81]. However, to use magnetic nanoparticles in suitable biomedical applications, the surface chemistry of magnetic nanoparticles is required. In general, the pure magnetic nanoparticles incline to aggregate into large clusters due to their large surface area-to-volume ratio and dipole-dipole interaction. Therefore, surface modification of magnetic nanoparticles provides both preventing aggregation of them and enhancing their water solubility, biocompatibility, bioconjugation, and nonspecific adsorption to cells.

There are different methods for synthesis reported in the literature can be classified into four main groups. Namely: co-precipitation, microemulsion, thermal decomposition and hydrothermal synthesis [87].

Co-precipitation is a simple and convenient way to synthesize iron oxides (both of Fe_3O_4, γ-Fe_2O_3) by using iron salts where the bases are added to aqueous iron solutions at room temperature or elevated temperature. Co-precipitation is a simple and convenient way to synthesize iron oxides (both of -) by using iron salts where the bases are added to aqueous iron solutions at room temperature or elevated temperature. The

size and shape of magnetic nanoparticles depend on the types of salt used, pH and temperature. This method especially is employed to produce the small size of beads, which have a diameter length of less than 50 nm.

Thermal decomposition is a chemical decomposition technique that used to synthesis of high-quality semiconductor nanocrystals and oxides in non- aqueous media by heat. Magnetic particles with a smaller size can be synthesized in through the thermal decomposition of organometallic compounds in boiling organic solvents containing a suitable stabilizing surfactant.

The microemulsion is a definition of a thermodynamically stable dispersion of two mixtures of immiscible liquids. This method can be used as a reactor for forming nanoparticles. It is especially used to synthesize metallic cobalt, gold-coated cobalt/platinum nanoparticles. Although many types of magnetic nanoparticles have been synthesized by microemulsion, the particle size and shapes are very over. Thus, it is not a very efficient method compared to other methods.

Hydrothermal synthesis is used to synthesize a broad range of magnetic particles. The system consists of solid, liquid and solution at different reaction temperatures under hydrothermal conditions. It is based on a general phase transfer and separation mechanism occurring at the interworking of solid, liquid and solution phases during the synthesis. In this way, magnetic particles can be synthesized with tunable sizes in the range of 200–800 nm.

Although there are several methods for synthesizing magnetic nanoparticles, the encapsulation part is also crucial for their stability and protection for long-term utilization. Stability is the most important property for magnetic particles to employ almost any applications. Thus, the protection of them is necessary by a layer, which is impenetrable, so that oxygen cannot react to magnetic particles. The protection method base on a core-shell structure that shells isolating the core material against to environment cover magnetic particles. The coating strategies are mainly divided into two categories: coating with organic shells, including polymer and surfactant or coating with inorganic materials: including carbon, silica, and metals e.g. Ag, Au.

Following encapsulation, the functionalization of the magnetic particles is also necessary. They are functionalized with a specific component such as specific binding sites, species, various drugs, or other functional groups. This step provides magnetic particles to be easily separated and controllable by an external magnetic field.

2.2.4 Detection Techniques of Magnetic Particles

After binding the magnetic particles to biomolecules as a biomarker, the final step is the detection of magnetic particles. Nowadays, sensor technology in biological and biomedical applications has been earning important attention and development. Therefore, wide ranges of detection techniques for the suitable applications have been used to measure the response of the magnetic particles. Using these techniques one or more parameters can be measured. Some of them are explained below.

2.2.4.1 Spintronic Sensors

There are three types of magnetic detection techniques that are giant magnetoresistance (GMR) sensors, tunneling magnetoresistance (TMR) sensors and planar Hall Effect (PHE) sensors.

Giant Magnetoresistance sensors have been used as a magnetoresistance based solid-state sensors. Among other types of sensing methods, the spin-valve is the most common and effective technique with small sizes of magnetic participles. Spin valve sensors are composed of an artificial structure with alternating ferromagnetic and nonmagnetic layers. These types of sensors measure the magnetoresistance effect, which is produced by moving electrons between the spin-orbital couplings. When an external magnetic field is applied, it rotates the magnetic layer towards alignment and spin-dependent electron scattering is reduced at the interfaces within the device, thus the electrical resistance is measured. GMR sensors are microscopic in size and they are very sensitive to detect micron and smaller size magnetic particles. They are commonly employed in data recording, like magnetic random access memory (MRAM) [88], for immunoassays in a manner enzyme-linked immunosorbent assays (ELISA) [89], DNA-DNA interactions and protein immune-sensing and for multiple detections [79].

Tunneling Magnetoresistance sensors are based on the tunnel magnetoresistance of a magnetic tunnel structure that consists of two parallel magnetic layers and an insulating layer. TMR sensors prove a higher magnetoresistance ratio than GMR sensors, which means they have higher sensitivity at low magnetic fields [90]. They have been employed to detect DNA hybridization [91], for immunoassays to detect liver cancer biomarker [92] and for the detection of small particles of iron oxide magnetic particles used in environmental applications [93].

Planar Hall Effect sensors have been employed for the detection of micro and nano-sized magnetic particles. The design of these devices based on the measurement of the planar Hall effect of ferromagnetic materials. They measure the change in anisotropic magnetoresistance caused by exchange-biased permalloy. A study of exchange biased PHE sensor provide that they have high stability between -10^oC and -70^oC temperature in biomedical applications [94]. There have been studied to improve their architectures to gain higher signals in biosensing applications.

2.2.4.2 Nuclear Magnetic Resonance (NMR)

Nuclear Magnetic Resonance is a strong magnetic phenomenon, which is used for identification, detection and imagination of molecules. NMR sensors measure an entire volume of the sample unlikely other detection techniques GMR, PHE, TMR, and SQUID (Superconducting Quantum Interference Device), is explained in the next section [95]. NMR detection techniques are based on the measurement of the nuclear relaxation difference induced by the magnetic field of magnetic particles. They provide the information of magnetic particles that the higher transverse relaxation rate which means the higher concentration of magnetic particles. One of the most significant applications for magnetic particles based NMR devices are magnetic resonance imaging (MRI) of detected magnetic particle labeled molecules. Magnetic particles used in MRI play two roles both specific tags and contrast agents, thus they provide a non-invasive molecular level imaging method. There are a lot of reviews in the design and functionality of magnetic particles in MRI with applications widening from the molecular level to the organ level [96]–[98]. In addition to MRI based magnetic particles, there are microsystem NMR sensors, which provide point-of-care detection and they can be integrated with microfluidic systems like [99].

2.2.4.3 Superconducting Quantum Interference Device (SQUID)

A SQUID is the most sensitive magnetometer used to measure very subtle magnetic field based on the superconducting loops including Josephson junctions. When an external magnetic field applied, it induces the current in the device and voltage change occurs across the junctions, which generates an output signal. The output signal is transformed into magnetic flux and the output information is given. The most magnetic particle-based detection sensors measure the magnetic field difference

produced by the magnetic particles. The SQUID based biosensors are classified into three main types: relaxation-type, remnant-type, and susceptibility-type sensors.

Relaxation type sensors based on the measurement of bound magnetic particles and unbound magnetic particles response after the absence of an applied external magnetic field. In the case of them, the bound magnetic particles relax (Neel relaxation time) at a slower velocity than the unbound magnetic particles (Brownian relaxation time). Therefore, the SOUID sensor measures the response of the magnetic responses for both bound and unbound magnetic particles after switching off the applied magnetic field. These types of sensors are employed to detect kinetic studies of antibody-antigen reactions in whole blood samples [100].

The remnant type sensors are also based on the measurement of unbound magnetic particle response in the absence of an external magnetic field after exposing magnetic particles to a magnetic field. In this case, the bound and unbound magnetic particles are distinguished on a surface without requiring any prior separation process and the unbound magnetic particles are removed. The remnant sensors are non-invasively used to track and identify the magnetic particles in human organs [101].

Magnetic susceptibility methods are used for the magnetic particle identification and immunomagnetic reduction mechanism like [102]. SQUID sensors are also used in MRI, detecting magnetic particle agglomerations.

2.2.4.4 Atomic Magnetometer (AM)

Atomic magnetometer (AM) is a highly sensitive technique to measure DC magnetic field with an advantage of not requiring cryogenics, differing from the SQUID technique. The principle of AM based on the measurement of magneto-optical effect which is caused by a probing laser beam interaction with spin-polarized atoms in an applied magnetic field. Atomic magnetometers have been employed for the detection of magnetic particles in various applications. For example in [103], a single micro cobalt particle is detected by a microfabricated atomic magnetometer. Also, scanning imaging methods have been proven to detect magnetic particles. They provide spatial information and quantification of functionalized magnetic particles simultaneously. The imaging systems have been performed at physiological temperature, which is suitable for the study of biological samples using immunoassay. Moreover, AM is employed as

a magnetic relaxometry to detect biomedical samples like targeted MPs and targeted cancer cells [79].

2.2.4.5 Fluxgate Sensor

The fluxgate magnetometer is a magnetic field sensor, which measures the change in magnetic fields for a variety of applications from biomedical to archeology. The detection mechanism based on the magnetorelaxometry technique. These sensors provide the detection at room temperature and absolute magnetic fields compared to SQUID types relaxometer. They have been used for magnetic particle samples including Fe_3O_4 magnetic particles with or without a functionalized shell and magnetic particles used in the degradation of hydrogel. The micro-fluxgate sensors also have been used for the detection of magnetic particles in biosensing such as [104]. Furthermore, fluxgate magnetometers have also been employed to qualify the magnetization and relaxation dynamics of immobilized Fe_3O_4 magnetic particles [105].

2.2.4.6 Frequency Mixing Magnetic Detection Techniques

These frequencies mixing magnetic detection biosensors are based on the detection of nonlinear magnetic materials. In this case, magnetic fields of two different frequencies are employed to label magnetic material, which gives a nonlinear magnetic response. The response detection provides to signal the presence of magnetic particles. This technique is specifically used or the application of superparamagnetic materials due to their nonlinear magnetic properties. It has been used for the detection of many biological species [106]. In this study, planar-frequency mixing magnetic detection is employed to acquire 2D images of superparamagnetic particles for the detection of early-stage of Alzheimer's disease.

2.3 Signal Amplification Methods in Biosensors

Developments in the life science and biomedical science bring about new biosensor applications mainly focus on the detection of low abundance and the acquisition of low signals. Although there are various sensitive signal detection techniques, the signals acquired from biosensors are often required amplification.

Improvements in micro/nanotechnology open up signal amplification methods for biosensors [107]. Signal amplification methods in biosensors mainly can be divided into three groups: nucleic acid-based signal amplification, enzyme-based signal amplification, 1-to-N binding based signal amplification [108].

2.3.1 Nucleic Acid Based Signal Amplification

Nucleic acid-based signal amplification provides to use small numbers of biological samples to diagnose molecules that are commonly used in the recombinant DNA technologies and molecular biology. The combination use of DNA amplification for protein detection provides to achieve high sensitivity when analyzing cancer target biomarkers, infectious diseases, and biochemical processes. Polymerase Chain Reaction (PCR) based signal amplification, isothermal nucleic acid amplification, and enzyme-free nucleic acid amplifications are the main categories for this amplification method. Some example of them is given below.

2.3.1.1 PCR Based Signal Amplification

PCR is one of the common methods for signal amplification due to its high sensitivity and good reproducibility. It is based on the detection of an antibody-antigen reaction. However, instead of using an enzyme-conjugated antibody, the antibody labeled with a DNA fragment is amplified by utilizing PCR method through pairs of primers. The amplification successes of PCR open up to produce large amounts of DNA products that can be detected by many methods.

2.3.1.2 Isothermal Nucleic Acid Amplification

There are several isothermal amplification methods without using a thermocycler machine such as helicase-dependent amplification (HDA) and rolling circle amplification (RCA). These methods have been provided according to the new findings in molecular biology DNA/RNA synthesis.

RCA is an enzymatic process that requires a circular template and a primer, which extended via DNA or RNA polymerase resulting in long single strained DNA (ssDNA) consisting of a complement of the circular template. This long chain provides to link DNA detection probes, which can be detected by several methods. Aiming at the

detection and capturing platelet-derived growth factor B-chain (PDGF-BB), which is known to relate to tumor growth and transformation, and the amplification problem is solved by PCR and magnetic beads [109]. Lee at al. provided an aptamer-based sandwich assay performed on micro contact-printed streptavidin-coated magnetic beads that conjugated to biotinylated probes, which bound to RCA. Thus, for the amplification method, RCA and magnetic beads were used as a hybrid system.

2.3.2 Enzyme Based Signal Amplification

Using enzymes in catalysis is the most widely used method for signal amplification. The enzymes used in proper biosensing applications conjugated to target molecule and produce colored, fluorimetric, or luminescent signals, which can be detected by various methods. This method has been used in the enzyme-linked immunosorbent assay (ELISA) that is commonly used to bind the presence of target molecules.

In the enzyme-based signal amplification method, natural protein enzymes DNA enzymes, nano enzymes, and nucleic acid enzymes are employed according to the desired detection and enhancement process [108].

2.3.3 1-To-N Binding Based Signal Amplification

Biotin–streptavidin system (BAS) and nanocarriers are used in this method for the amplification of signals. In BAS, the binding properties of streptavidin's subunits, which conjugate to biotin, exhibits high-affinity protein-ligand interactions so, the signal amplification is achieved.

The achievements of nanotechnology and nanoscience provide nanomaterial-based signal amplification to hold great promise in detecting high sensitivity and selectivity for in situ or online detection of biomolecules due to the rapid analysis procedure and easy miniaturization. A lot of nanomaterials are effective candidates for being nanocarriers in signal amplification because of their unique properties such as high binding surface area. The resulting conjugation of nanoparticles with biomolecules equipped the abilities both recognition of target molecules and signal amplification [110].

2.3.4 Magnetic Accumulation Based Signal Amplification

Although there are many kinds of signal amplification methods, the magnetic accumulation based signal amplification method is novel and it has advantages compared to other methods. In this method [111], different types of uncoated magnetic beads such as ferromagnetic, paramagnetic and superparamagnetic beads are used, which are cheaper than coated magnetic beads, they can be controlled by an external magnetic fields and they can easily bind based beads and amplify the signal captured from target analyte.

In this work, the effect of magnetic beads types and size, the effect of the magnetic field and accumulation dynamics of magnetic beads are measured to provide signal amplification strategy. Finally, the technique is supported by an experiment that E-coli cells are used as a target and captivates immunomagnetic beads are used as base beads, which bind the E-coli cells. The uncoated magnetic beads are added to E-coli captivate bindings solution and they bind immunomagnetic beads and amplify signals [112].

2.4 Diffraction Gratings

Biosensing is a crucial method for biosensor applications in biomedical science. There have been several methods to capture target biomolecules using biomolecular probes such as antibody, aptamer, DNA, and proteins [31]. One of the methods to pattern the probes is the micro-contact printed lines method [109], [113], [114]. Using micro-contact printing on the gold surface as a probe proves high binding to biomolecules. The immunomagnetic beads are employed on micro-contact printed lines due to their target capture and separation features for labeling and transferring the target molecules.

Micro-contact printed lines or called diffraction gratings based sensors have been developed by incorporating with biomolecules. For example, Chang et al., [113] developed reflective diffraction gratings by incorporating hydrogels as a biochemical sensor. The hydrogel is a reversible swelling characteristic material, which is affected by pH changes. When the pH value of the aqueous environment increases, the hydrogel swell and when it decreases, the hydrogel shrink. Here, the detection mechanism based

on detecting the phase of gratings, which is fabricated from a biochemically responsive hydrogel that is induced only by the change of grating heights. In this study (Acharya et al) [114], the micro fabricated optical diffraction biosensor is described for the rapid detection of S-adenosyl homocysteine (SAH), which is a diagnostic biomarker of cardiovascular disease. Using PDMS (poly-dimethylsiloxane) stamp with 15−μm-wide pattern for microcontact printing, aptamer micropatterns were deposited on the gold chips. BSA (bovine serum albumin) is used to block the free stripes and the gold chips incubated in BBSA (biotin conjugated bovine serum albumin) for high affinity binding. The gold chips containing BBSA micro-contact printed pattern were dipped in streptavidin solution. Then, the gold chips were exposed to a suspension of SAH–Ab beads to produce grating patterns using aptamer SAH-Ab beads binding. The produced diffraction gratings are given to clarify the method in Figure 2.4.1. For detecting diffraction gratings, a laser was used to illuminate the micro pattern that gave the characteristic of the diffraction grating.

Different methods have been employed to quantify the binding biomolecules on micro-contact printed lines such as atomic force microscopy (AFM), fluorescence microscopy, optical microscopy and X-ray photoelectron spectroscopy (XPS). However, these quantification methods are costly and they require experts and high-quality equipment.

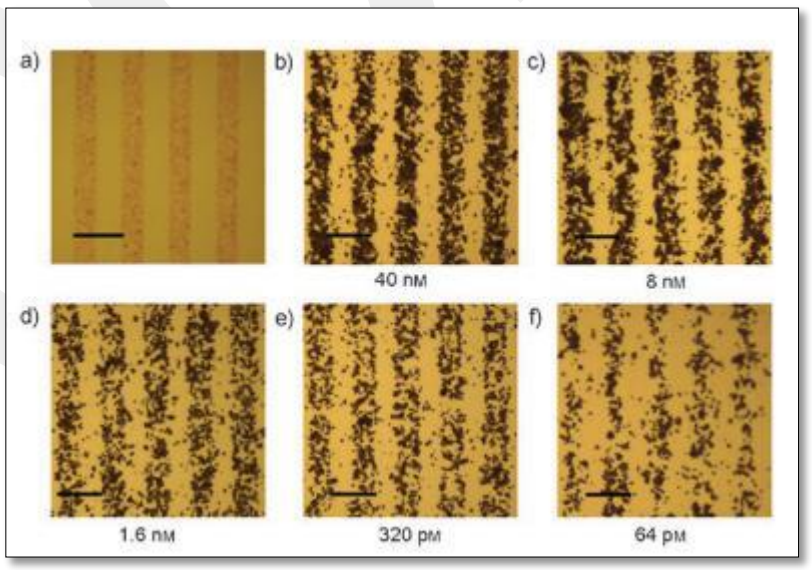

Figure 2.4.1 Diffraction gratings for detecting of S-adenosyl homocysteine using SAH-Ab beads. Scale bar is 30μm [114]**.**

Chapter 3

3 Methods

In this chapter, the methods of our work will be explained. Firstly, we used image processing based detection for quantification of Acute Lymphoblastic Leukemia (ALL) cells and magnetic beads in microscopic images taken from an optical microscope. The methods of image processing that are used for both optical microscopy and cell phone microscopy will be clarified with the example of the literature search. Secondly, the cell phone microscopy technique for diagnostic imaging and our experimental set-up will be given.

3.1 Image Processing Based Detection

A digital image is composing of a finite set of pixels in two-dimensional plain, that every pixel has a value. In grayscale images, a pixel has an integer value between 0 and 255 called an 8-bit pixel value, which represents 2^8=256 values. For color images, a pixel is consisting of three-dimensional integer vectors that each vector represents a color red, blue and green. These component values lie generally between 0 and 255, which is called 24-bit RGB color image (24=8x3[RGB]) [115]. In this work, any RGB color image is assumed to have 24-bit RGB and the grayscale image is assumed to have an 8-bit grayscale. However, there are many image variations in grayscale and color images representations [116].

RGB images are generally converted to grayscale images for image processing methods according to the application of bioimages. The main way of converting an RGB image into a grayscale image is that RGB image pixels have triplet values corresponding red, green, blue color components are specified in spatial locations to a single value by calculating the weighted sum of each color component.

3.1.1 Binarization

Binarization is a method to convert original grayscale images into black and white images, which has the pixel value 0 and 1, respectively. Binarization is mainly used to separate bright target objects from a dark background or vice versa. The resulting black and white images have connected white-pixel regions and black-pixel regions that each of the regions is called connected components. The white connected components provide to gather information from target objects such as number, shape, size, and area by analyzing the white connected components values. For example, the circularity of a single object can be analyzed. In this case, binarization can be considered as a segmentation method. There are three main types of binarization methods: global thresholding, local thresholding, and optimization-based binarization, which are explained below.

Global thresholding is the binarization method, which is based on the determination of a threshold value. In this method, the threshold value is the same for each pixel of an image that the pixels have a gray level value. If the values are bigger than the threshold, they are converted into white. If the pixels have smaller values than the threshold, they are converted into black. The global thresholding assumes that the gray level distributions are constant over the image.

Otsu's method [117] is the most famous global thresholding based on the determination of a threshold value which is calculated automatically by using the discriminant criterion. In this method, the histogram of the images is divided into two main parts. For example, if the image has uniform between the brightest (255) and darkest (0) gray values, which means the histogram is uniform, the threshold value is selected at the middle value.

Local thresholding is generally used when the background of the image has brighter values than some target regions. In this case, the global thresholding is insufficient having the constant thresholding. Local thresholding overcomes these types of backgrounds by combining two global threshold values as shown in Figure 3.1.1.1. It selects an optimum binarization threshold at each pixel. An example of this thresholding, Niblack's method [118] determines a threshold value x which is a sum of an average pixel value of a small region and its small negative values.

The optimization-based binarization method deciding each pixel belongs to black and white depend on neighboring pixels, which is an optimal decision problem called

Markov random field (MRF) [115]. For an MxN image, there are 2^{MN} possible decisions according to MRF. Thus, it is time consuming and inefficient method for biological images.

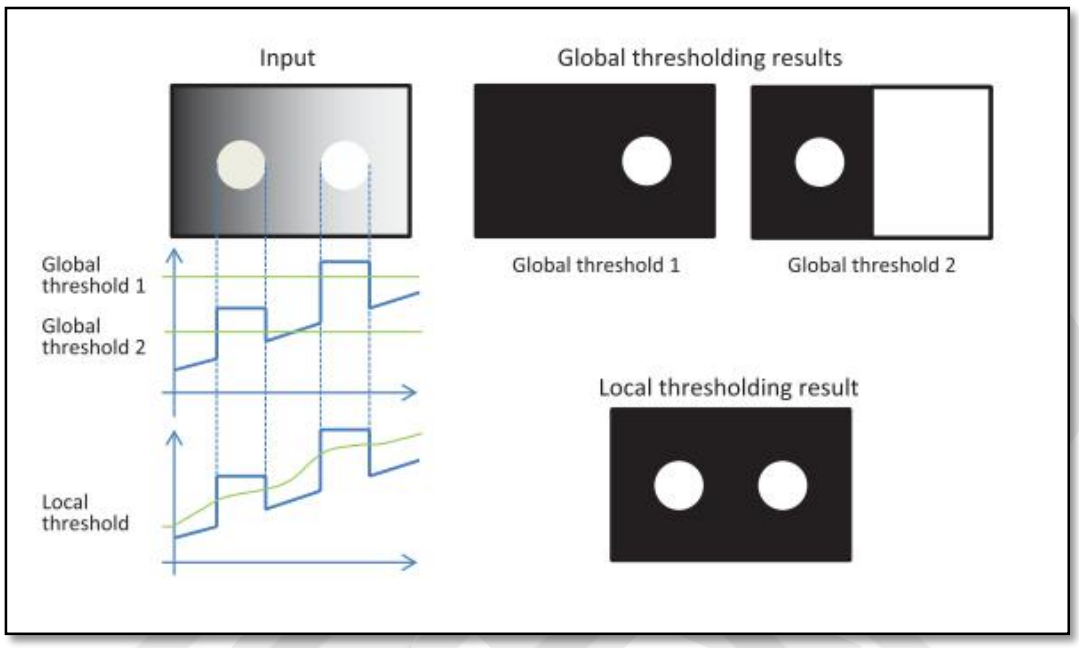

Figure 3.1.1.1 It is an example of the local thresholding sets the threshold value by combining the local thresholding around objects [115]**.**

3.1.2 Image Filtering (Mean Filter)

Image filtering is commonly used for the first step of image processing methods. In some applications, images are needed filtering for further processing steps and the input image is converted to another image with different values due to filtering. There are two main types of image filtering techniques: linear filtering and nonlinear filtering. If the computation of neighboring pixels is linear, the method is called linear filtering otherwise it is called non-linear filtering.

Although there are many types of image filtering methods, in this thesis the average/mean filter is employed for the pre-processing of magnetic beads detection of diffraction gratings explained in 4.2.

A mean filter is based on replacing the original pixel value by the mean pixel value around the pixel. When the average filter cancels noise, the ultimate image

becomes smooth. Assuming a one-dimensional image has the pixel values (9, 12, 9, 10, 8, 10). Averaging among these pixels with two neighborhoods, the pixel values become 10.5, 10.0, 10.3, 9.0, 9.3, 9.0). As explained by this example, the differences between pixels can be minimized which smooth the image.

3.1.3 Morphological Operations

In image processing, the morphological operations are employed to extract meaningful information from the target objects based on properties of form or shape inside the image. They are commonly applied in segmentation applications for automated counting and detection. Although they can be applied all types of images, they mainly utilize for processing of binary images [119].

3.1.3.1 Structuring Elements and Neighborhoods

A structuring element is a rectangular shape of pixels array consist of the pixel values 0 and 1 that resembles a small binary image. Some examples of structuring elements are illustrated in Figure 3.1.3.1.1.1.

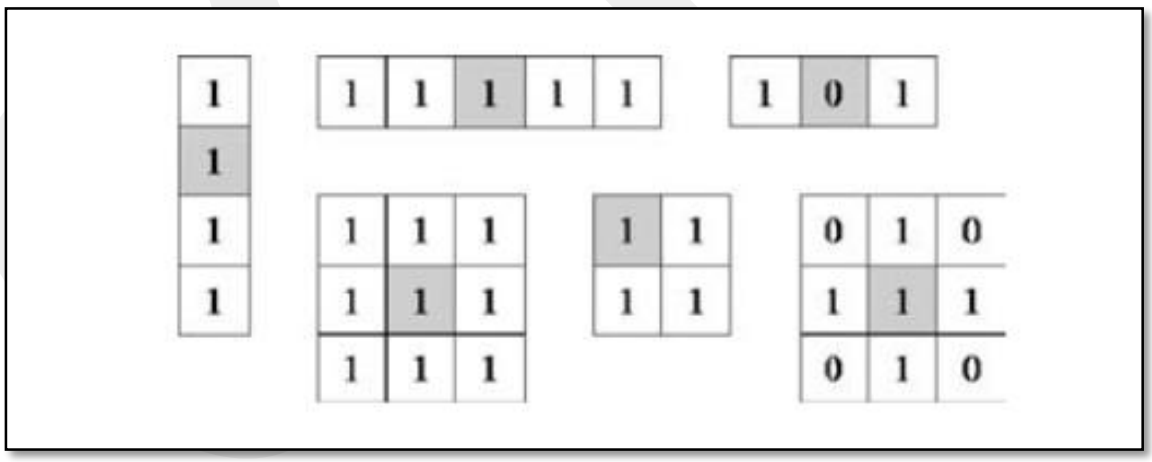

Figure 3.1.3.1.1 The images illustrates some of the example of morphological structuring elements and the shaded pixels represent the center pixel of structuring elements [119]**.**

A structuring element has a designated center pixel, which is located at the center when the structuring element has the same dimension called odd such as 3x3, 5x5. When the dimension is even such as 3x4, 5x6, the center pixel can be localized to north,

northwest or west. If the center pixel of structuring element is located directly above the pixel under consideration within the image, then the neighborhood of that pixel is designated by the pixels that lie under those pixels having value one in the structuring elements [116] as represented in Figure 3.1.3.1.2.

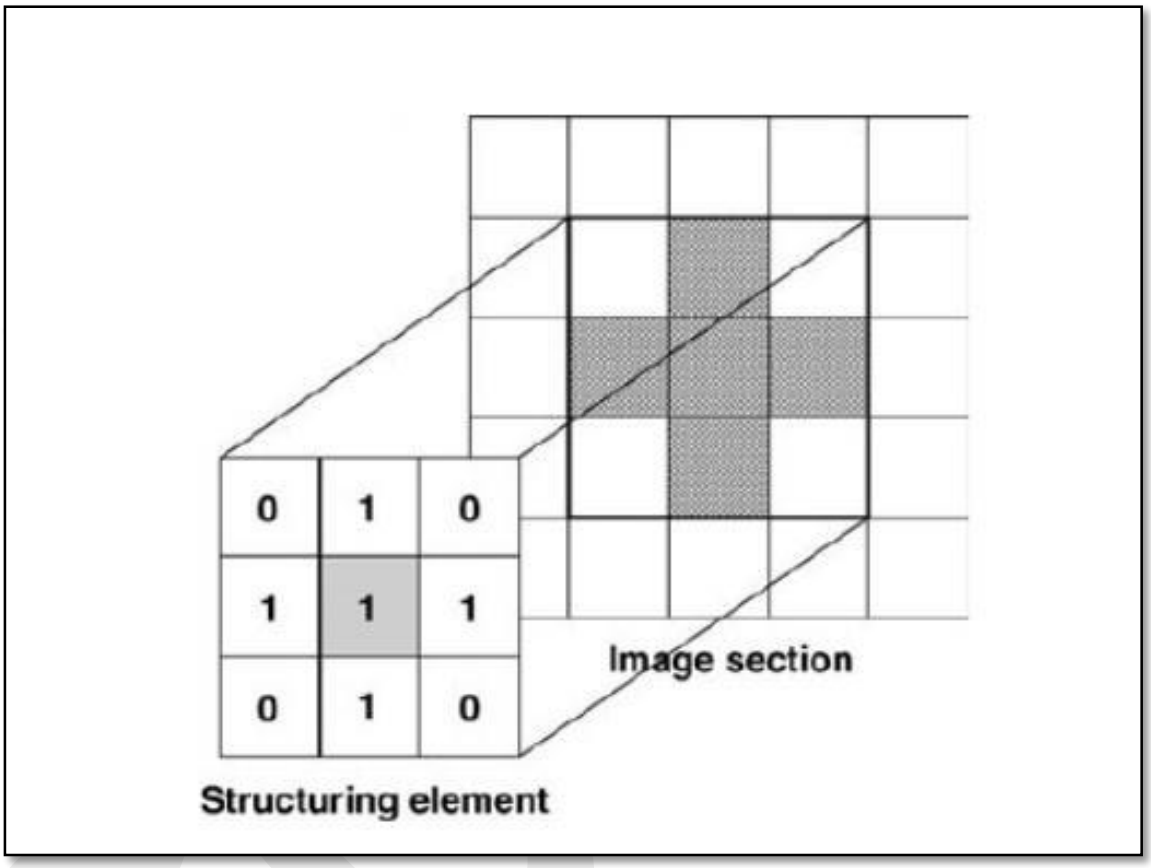

Figure 3.1.3.1.2 The local neighborhood determined by the structuring element. This is defined by those shaded pixels in the image, which lie under the pixel value having 1 in the structuring element [119]**.**

3.1.3.2 Dilation and Erosion

Erosion and dilation are the most significant morphological operators that other morphological operators can be derived in terms of the primitive of these two. The general image is denoted by A and random structuring element is represented by B, and erosion and dilation are denoted by A and B.

Erosion of a binary image is performed by applying a structuring element. The center pixel of the structuring element is placed on each foreground pixel that has value 1. If any of the neighborhood pixels are background pixel that has value 0, the

foreground pixel is replaced by background. In the formula, the erosion of the image A by structuring element B is represented A $\ominus$ B.

Dilation of a binary image is performed similarly to erosion. The center pixel of the structuring element is placed on each background pixel. If any neighborhood pixels are the foreground, the background pixel is replaced by the foreground. Formally, the dilation of image A by structuring element B is represented A $\oplus$ B [119]. An application of dilation is illustrated in Figure 3.1.3.2.1.

In application, it can be briefly said that dilation increases the size of binary objects and erosion decreases the size of binary objects. Dilation and erosion operators are the reverses of each other.

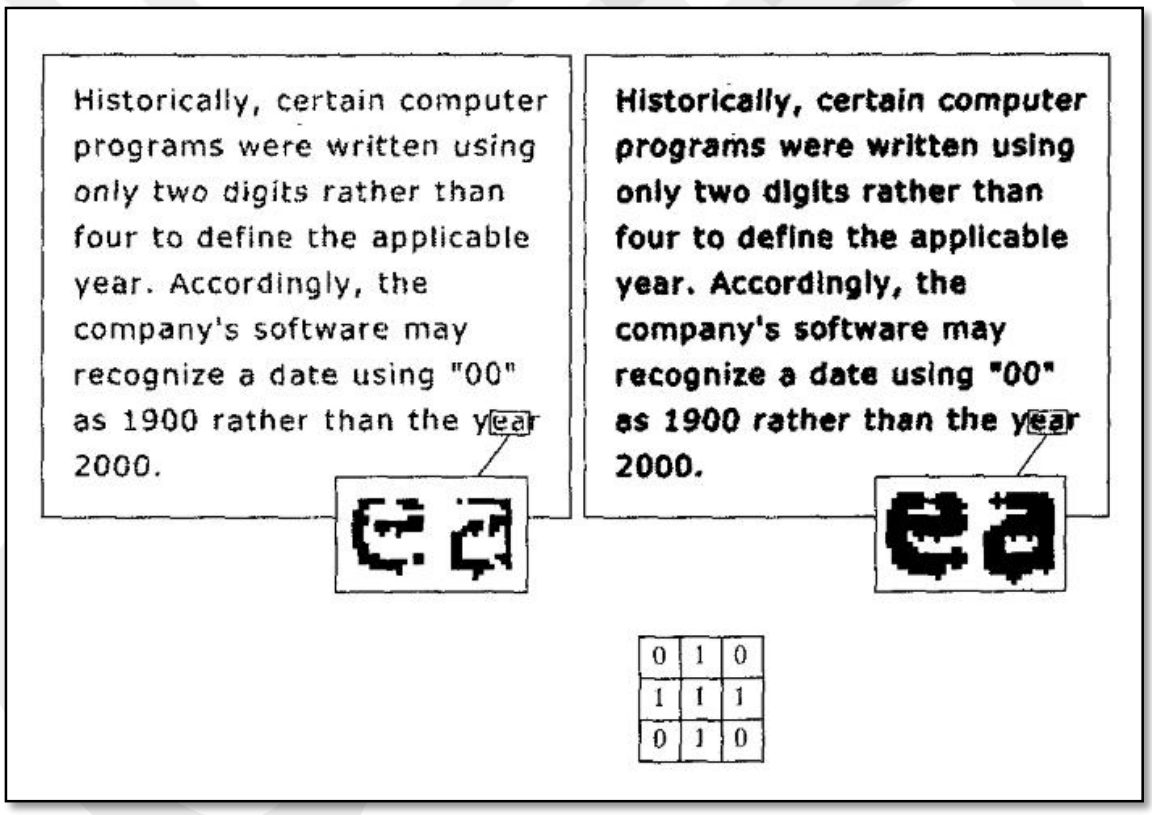

Figure 3.1.3.2.1 It is an example of a dilated image. The left image is a sample image; the right image is the dilated image with represented structuring element below of images [116]**.**

3.1.3.3 Opening and Closing

Opening is a morphological operation that is provided by erosion followed by dilation using the same structuring element. It is donated the opening of A by structuring element B as $A \circ B = (A \ominus B) \oplus B$.

The general effect of the opening operation is to remove small objects from the foreground of an image, replacing them in the background.

Closing is a morphological operation that is provided by dilation followed by erosion using the same structuring element. It is donated the closing of A by structuring element B as $A \cdot B = (A \oplus B) \ominus B$.

The general effect of closing is removing small holes in the foreground replacing small regions of background into foreground [116], [119].

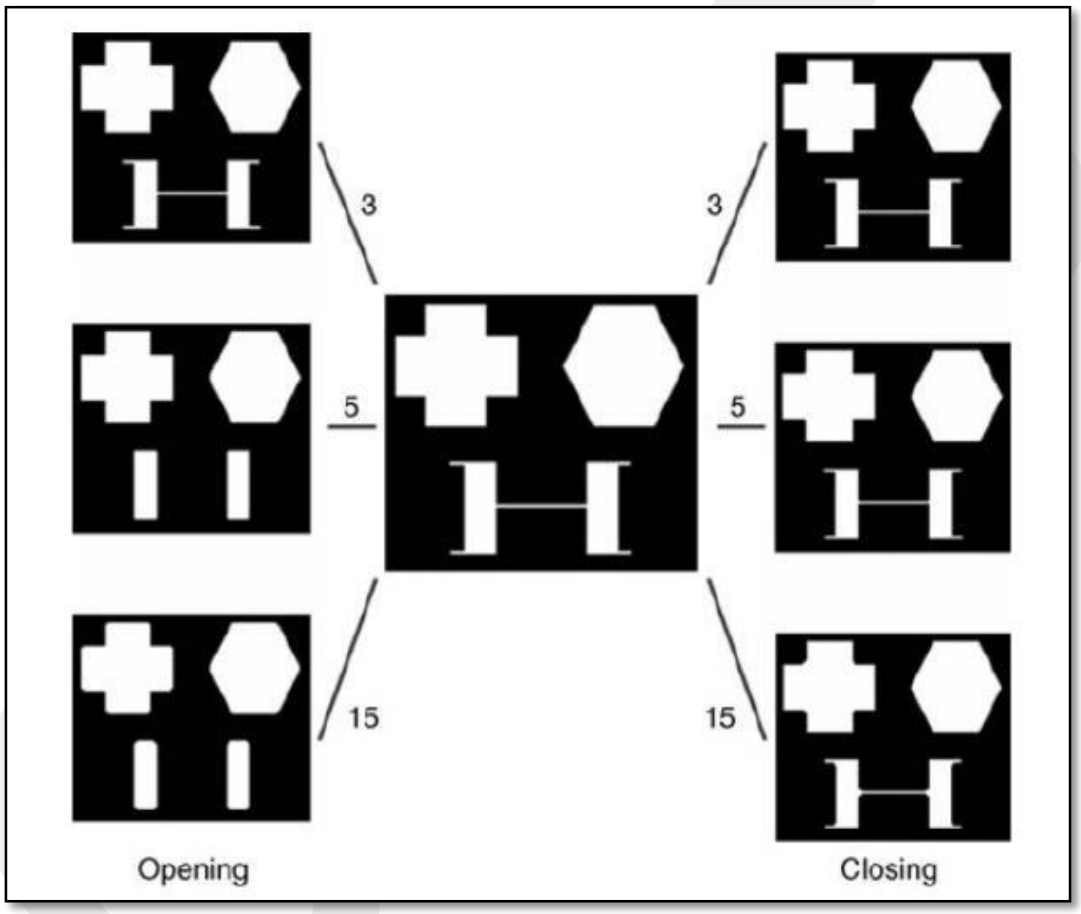

Figure 3.1.3.3.1 Illustration of the effect of opening and closing operations over some example shapes. The images to the left represent the opened original image placed in the center with structuring element has radii 3, 5, 15 top to bottom. The images to the right represent the closed original image with the structuring element has radii 3, 5, 25 top to bottom [119]**.**

3.1.3.4 Region Filling

Binary images generally occur in image processing applications as a result of thresholding and segmentation procedures as input grayscale images or color images. These procedures may leave some pixels or holes within the binary objects that require

filling. Region filling provides connections between these objects often desirable for subsequent processing procedures such as labeling, segmentation [119].

In MATLAB Image Processing Toolbox, the region filling is provided by imfill function [120].

3.1.4 Watershed Segmentation

The classical watershed algorithm [121] is based on flooding simulation as shown in Figure 3.1.4.1. Considering the grayscale images as a topographic surface, where the regional minimum values are assumed as valleys, the regional maximum values are assumed as peaks. When the surface is flooded by water, dams are erected among the valleys to prevent the flood. The union of all dams forms watershed lines, which are found by the watershed transform algorithm [12].

According to Meyer's algorithm [122], firstly regional minimum called 'valleys' are marked by selected different values and labeled them concerning the intensity values. Then, depending on the labeled intensity values, the neighborhood pixels of labeled areas are added to the priority queue with a priority rank. After that, the highest priority is selected among the priority queue. The selection of priority labeled areas based on the checking neighborhood pixels of the priority queue. If the labels are the same, the selection is repeated with another value. This election cycle is repeated until finding unlabeled intensity values, which called 'peaks' that are involved in watershed lines. The illustration of valleys and peaks are shown in Figure 3.1.4.1.

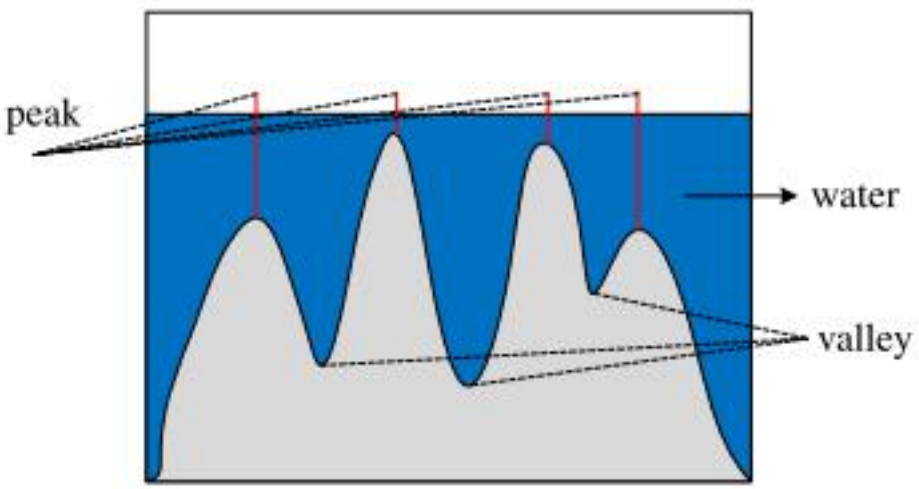

Figure 3.1.4.1 Watershed algorithm flooding simulation [12]**.**

3.1.5 Marker-Controlled Watershed Segmentation

The watershed algorithm is especially proper for the segmentation of close boundary or overlapping objects in question [12]. However, it may often deficient in over-segmentation as shown in Figure 3.1.5.1. Here, before segmentation, the morphological gradient applied to the original image. Watershed algorithm results in the over-segmentation.

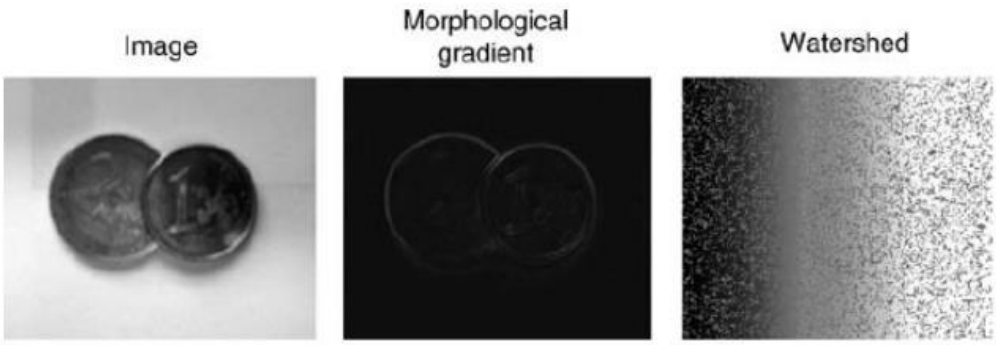

Figure 3.1.5.1 Direct application of watershed on gradient images often resulting in over segmentations [119]**.**

To overcome segmentation limitations, a standard watershed algorithm is strengthened with marker control. The basic instruction of the marker-controlled watershed calculation is that:

Firstly, select and calculate the ideal segmentation function. Dark regions (peaks) are the objects tying to be segmented. The modules of gradient images are usually chosen.

Secondly, process the original image to obtain foreground markers. Foreground markers are the connected blobs of pixels in each of the objects. This step is usually achieved by morphological operations.

Thirdly, marker background objects by repeating the process of morphological operations. Background markers are connected pixels of blobs, which are not parts of any objects.

Fourthly, process the segmentation function such as distance transform, regional maxima functions that it only process foreground and background markers locations.

Lastly, apply the watershed transform algorithm on the modified segmentation function [12], [15], [16].

An example of a marker controlled watershed algorithm is illustrated in Matlab Image Processing Toolbox and given here in Figure 3.1.5.2.

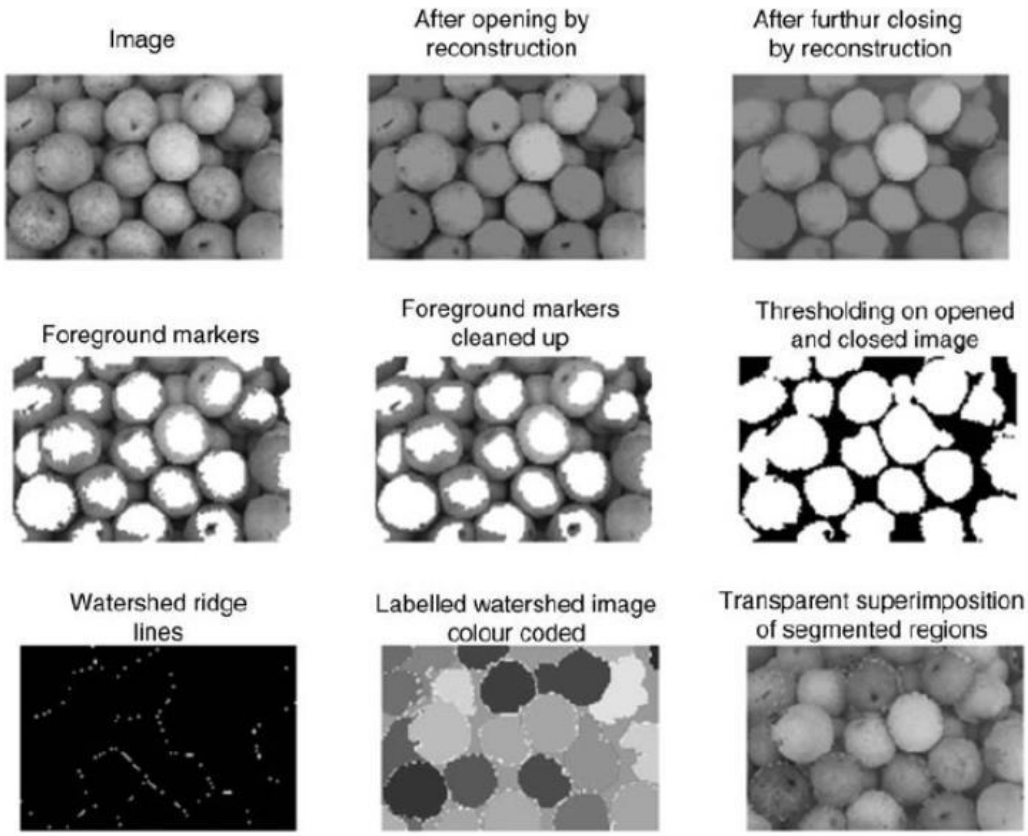

Figure 3.1.5.2 Marker controlled watershed segmentation given in Matlab Image Processing Toolbox [119], [123]**.**

3.2 Cell Phone Microscopy

An optical microscope is an essential tool in modern science and health care as well. The digital image diagnosis, analyzing and quantification are crucial for medical research. Although optical microscopes are widely used in clinical settings, they have some limitations. Firstly, a high-quality optical microscope and its objective lenses are expensive. Secondly, their field of view (FOV) is inversely proportional to the magnification factor that gives them the limitation of the diagnosis of the whole sample without mechanical scanning [123]. Additionally, their systems are complex; therefore they require a specialized person and they are inaccessible in rural and developing areas [124]. This is particularly a problem for the diagnosis, monitoring, and treatment of

diseases. To this end, several groups work on to provide novel methods of microscopic devices. The example of an optical microscope is shown in Figure 3.2.1 A.

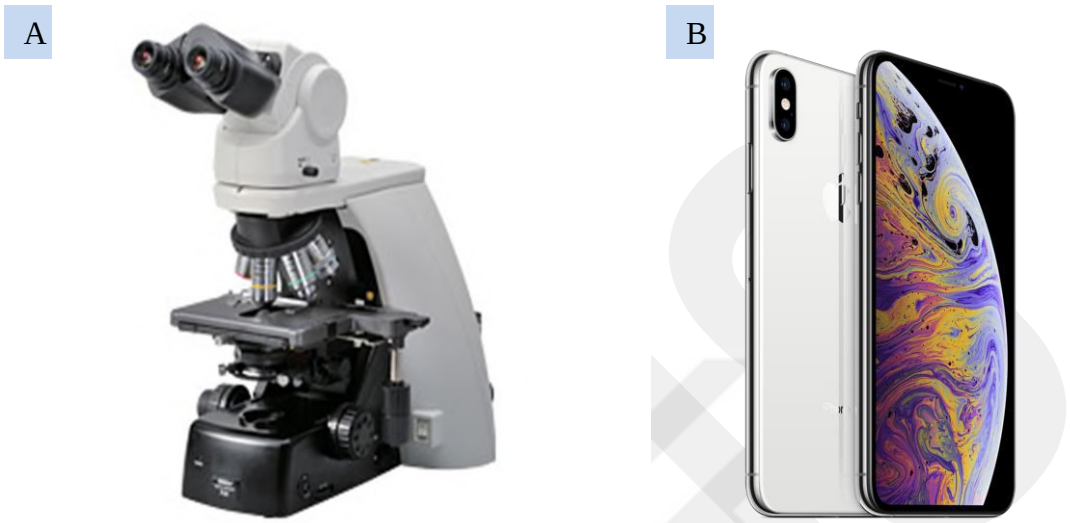

Figure 3.2.1 The illustration of microscopes (A) It is an example of an optical microscope [125]**. (B) It is an example of a new generation mobile phone which can be turned into cell phone microscopy** [126]**.**

Cell phone microscopy is gaining a significant role in clinical applications due to being low cost, portable, simple and the widespread use of mobile devices [127]. Today, they are similar to a miniature computer with high-quality memory, internet connection ability and having high-resolution camera lenses. They provide many opportunities in diverse areas being low cost and portable such as health care, environmental monitoring, and education. Furthermore, they open up the rapid diagnosis and analysis results for on-site point-of-care diagnosis [128], while also provide opportunities in general research [129]. An example of new generation mobile phone microscope is illustrated in Figure 3.2.1 B. Today, using advances in imaging technology, micro/nanoscale resolution can be achieved by cell phone microscopy for detection of nanoparticles, virus, DNA, blood cells, etc.

3.2.1 Related Works of Cell Phone Microscopy

Mobile phones have been transformed into microscopy by external attachments or accessories that use the advantages of mobile phone lenses or they can be transformed into a lens-free system. Several research groups have been working on a cell phone-based bioimaging system by using features of smartphones for images to quantify target samples. Breslauer et al., [130] demonstrated high-resolution microscope attachment for a camera-enabled mobile phone to screen hematologic and infectious diseases. The mobile phone microscopy system is capable of both bright field and fluorescence imaging. Furthermore, they provide simple image processing software to label and count the cells to improve diagnosing efficiency. The microscopy and imaging result illustrated in Figure 3.2.1.1 a. Also, other groups transform cell phones into microscopes [125]. Using high resolution camera and advanced computational capacity of cell phones, microscopic images can be recorded, calculated and process in real time, which allow to quantify features such as object sizes, shape, color and brightness as signal tags for healthcare diagnosis. Using a high-resolution camera and advanced computational capacity of cell phones, microscopic images can be recorded, calculated and process in real-time, which allows quantifying features such as object sizes, shape, color and brightness as signal tags for healthcare diagnosis. Furthermore, application program (app) can be created on mobile phones for capturing target biosamples and count cell numbers automatically as our feature goal explained in [124], [128], [131]–[137].

The optical attachments in the microscopic design are complex and sometimes costly due to microscope lenses. Despite having an optical attachment on mobile phones, some research groups are working on a lens-free microscopy system [136], which is shown in Figure 3.2.1.1 b. The system is called a compact and lightweight microscope that could be installed on a cell phone without any laser or lenses or other optical attachments. In this system, there is a lens-free imaging platform, which is attached to the cellphone camera and supported by an LED. Using this lens-free holographic microscope, they successfully image various sized micro-particles, blood cells such as red blood cell, white blood cells, and waterborne pathogens. However, the microscope has spatial resolution artifacts challenges, which is not enough to recognize nanoscale samples.

The spherical ball lenses are also used within mobile phones to convert them into a microscopy system. Bogoch et al., [134] demonstrate a mobile phone microscope that uses a spherical ball lens as a microscope lenses for the point-of-care diagnosis of soil-transmitted helminths. The system is easy to create, use and cheaper than creating a new stand or optical attachments, which is illustrated in Figure 3.2.1.1 c.

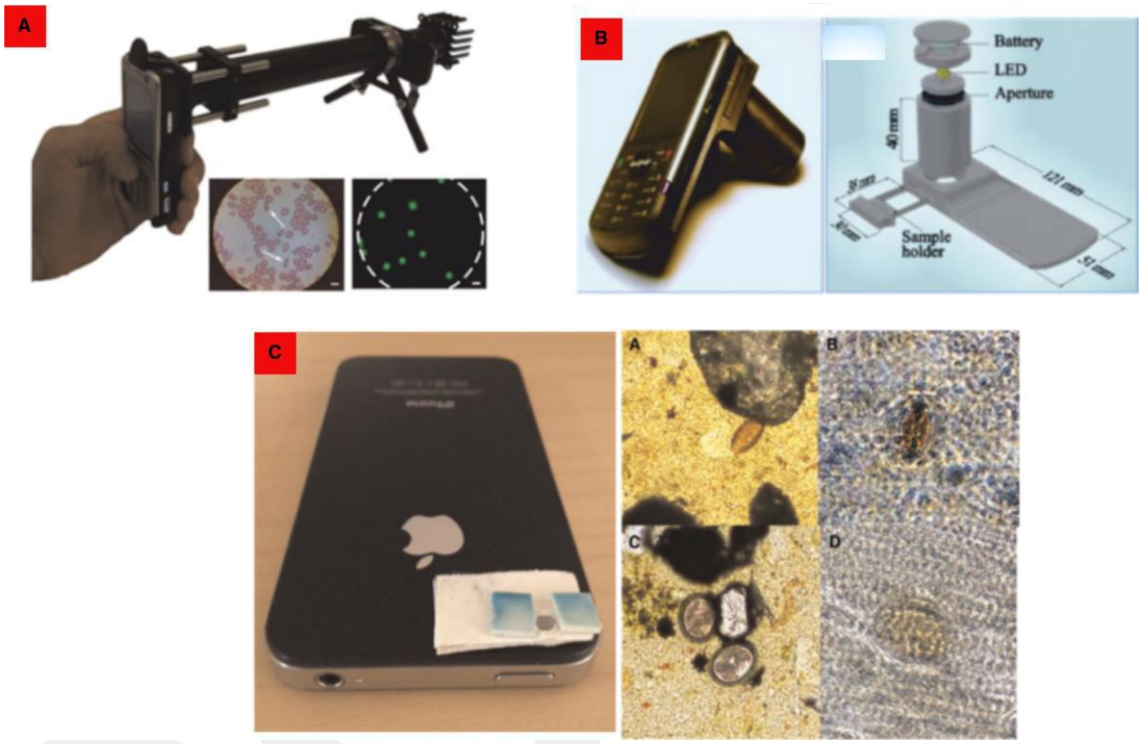

Figure 3.2.1.1 (A) A cell phone microscopy capable of both fluorescence and bright-field images created by [125]**; (B) The system is created with a microscopic platform and it is called compact and lightweight microscope** [136]**; (C) A mobile phone microscope that uses spherical ball lens as a microscope lenses for the point-of-care diagnosis of soil-transmitted helminths** [134]**.**

3.2.2 Our Cellphone Microscopy

In our work, the initial goal of creating a cell phone microscopy within a spherical ball lens, using the digital imaging capabilities and Internet connectivity to capture high-resolution microscopy images, and perform subsequent image transmission and analysis. The images are taken from optical microscopy Nikon (Melville, NY, USA) and cell phone microscopy Samsung Note 4 in the same area are shown in Figure 3.2.2.1.

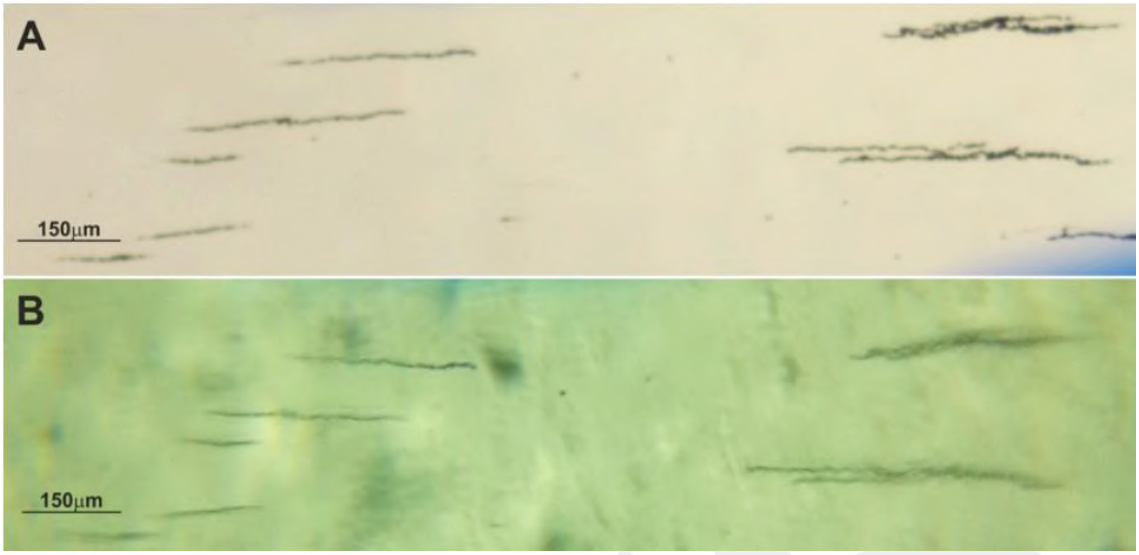

Figure 3.2.2.1 The illustration of the images recorded in the same area from optical microscopy and cell phone microscopy, respectively. (A) The image is taken from Nikon SE with 40x magnification. (B) The image is taken from cell phone microscopy using Samsung Note 4 with a spherical ball lens having 100x magnification.

The cell phone microscopy system consists of a Samsung Note 4 smartphone, borosilicate glasses spherical ball lens and a lens holder made by polymethylmethacrylate (PMMA) material as shown in Figure 3.2.2.2.

The cell phone is equipped with a 16-megapixel (5312 × 2988) camera composed of a Sony IMX240 imaging sensor and an f/2.2 lens with a 35 mm equivalent focal length of 31 mm.

To construct a lens holder, PMMA was purchased from Mc Master Carr (Elmhurst, IL, USA). PMMA was cut with a laser cutter as a lens holder as shown in Figure 3.2.2.2 B, then attached to the Samsung Note S4 cell phone with double-sided tape.

Figure 3.2.2.2 Cell phone microscope with a spherical ball lens. (A)Illustrates the crucial parameters of spherical ball lens; (B) The cell phone microscopy setup; (C) The measurement setup schematic.

The spherical ball lens was purchased from BioSpec (Bartlesville, OK, USA). There are some key parameters of spherical ball lenses must be clarified; Diameter of Ball Lens (D), Diameter of Input Source (d), Effective Focal Length of Ball Lens (EFL), Back Focal Length of Ball Lens (BFL), an index of Refraction of Ball Lens (n), which are illustrated in Figure 3.2.2.2 A. In our experiment, the spherical ball lens has a diameter of D = 3.51 mm and its refraction index of n = 1.517, which is made of borosilicate. By using these parameters, the images 100x magnified. The significant parameters of the spherical ball lens were calculated according to formulas [134] given in

Table 3.2.2.1;

Table 3.2.2.1 Parameters of spherical ball lens (all distance are in units of μm) [138]**.**

Parameter	Formula	Calculated Values
Magnification	$\mathrm{MAG} = (5x10^5 \mu m)^{\frac{2(n-1)}{nD}}$	97.1
Effective Focal Length	$\mathrm{EFL} = \frac{\mathrm{nD}}{4(\mathrm{n}-1)}$	2575
Back Focal Length	$\mathrm{BFL} = EFL - \frac{D}{2}$	820
Numerical Aperture	$\mathrm{NA} = \frac{2\mathrm{n}(\mathrm{n}-1)}{\mathrm{nD}}$	0.18

When the spherical ball lens with lens holder attached to the cell phone, another flashlight was used below of the sample to record images as shown Figure 3.2.2.2.

This experimental setup was used to capture images from the microscopic glass slide and diffraction grating-based biosensors. The images taken from microscope slides were processed by using image-processing methods and will be explained in 4.1 and the result of diffraction gratings' images will be explained in 4.2.

Chapter 4

4 Results

In this chapter, the results of our work based on an image processing method will be explained. Firstly, magnetic bead detection from cell phone images will be given with the experimental set-up, image-processing methods and the obtained results. Secondly, magnetic bead detection on diffraction gratings will be explained similar to the first section. Finally, magnetic bead and cell detection for microscopic images will be stated.

4.1 Magnetic Beads Detection from Cell Phone Images

In our work [139], we provide a signal amplification method for biosensing applications using magnetic beads based on the accumulation of them. In this method, a mobile device and simple spherical glass lenses are employed as a low-cost microscope for the detection of magnetic beads. Magnetic beads have two major roles in biosensing applications: First, they capture, separate and transport target biomolecules. Second, they attract other magnetized particles and form them under an applied external magnetic field. When a magnetic field is applied, magnetic beads accumulate and form a cluster. Thus, the corresponding pixel area of the cluster in the taken image by the cell phone microscope is increased.

In this work, the experimental setup is established for the detection and the quantification of magnetic particles from cell phone images. The method proposed in this section has four main components.

First, the immunomagnetic beads are used for capturing the target biomolecules. The solution of immunomagnetic beads is prepared for biosensing application as explained in our previous work [111].

Second, the uncoated magnetic particles such as ferromagnetic particles, superparamagnetic particles, and iron nanoparticles are used for signal amplification.

The selected magnetic particles are added to the solution of magnetic beads for the signal amplification. Then, the solution dropped on the glass slide under a suitable external magnetic field, for this work 16 mT, for the desired application.

Third, the cell phone microscopy system is employed for recording images. The system composed of a Samsung S4 cell phone, borosilicate glasses spherical ball lens and a lens holder made by polymethylmethacrylate (PMMA) material. The system is detailed in section 3.2 Cell Phone Microscopy.

Lastly, the image-processing algorithm is applied to the images recorded from the cell phone. The recorded images might be noisy and their resolution might require enhancements. To filter and quantify images, the image processing part is necessary. The image is sent to the cloud server, cloud server run the codes and ask the user which information wants to obtain and shows the chosen results to the user. Cell phone microscopy-based image processing that we used is shown in Figure 4.1.1.

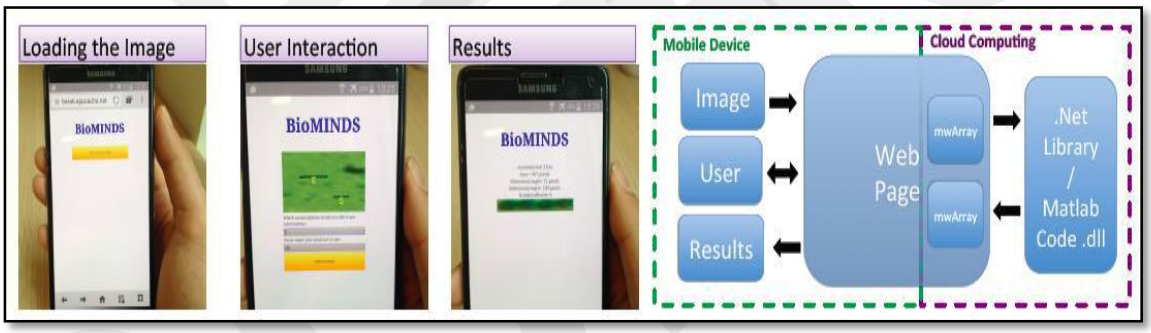

Figure 4.1.1 Cell phone microscopy based on image processing with cloud server.

In this work, Matlab Image Processing Toolbox (Version 2014b) is used to process recorded images. The image-processing algorithms of magnetic beads detection and quantification method of steps are explained below.

Step 1: Given an RGB image as the input, the binarization process started with pre-processing to label each of the accumulated magnetic beads. Firstly, the RGB image was converted to the grayscale to obtain a binary image. The original image and the grayscale image are illustrated in Figure 4.1.2 a and b, respectively.

Step 2: The binarization of the image was obtained by using the mean and standard deviation approach rather than Otsu's method [111]. When Otsu's method applied, most of the information about the image was got lost. However, in our approach, the mean of the grayscale image gives the average of the image's histogram

values. The subtraction of mean and standard deviation from the grayscale image gave the binary image, shown in Figure 4.1.2 c.

Step 3: After obtaining a binary image, morphological operations were employed to filter background noises acquired because of ball lens demerits. To overcome this challenge, imclearborder and bwareaopen functions were used to clear border and background noises. However, the background noise still needed filtering, so the next steps were applied to filter them, Figure 4.1.2 d.

Step 4: In this step, the aim is to clear small objects, which is not an accumulated beads chain, to detect accumulated beads. To success this, the regional property features were used. Initially, imfill function was used to fill the binary holes that are obtained in the previous step, and then labeled all filled holes finally, all of the regional properties obtained by regionprops function.

Step 5: Here, to clear small objects from the image, the area information of holes were used. All of the areas of the holes were obtained and the mean of area value was found. Then, the areas smaller than average were cleared by using ismember function.

Step 6: Now, we had only information about bigger holes that can be called the accumulation of magnetic beads aims to be detected. To show the detected accumulation of magnetic beads, big holes information was gathered by regionprops function, and then founded the boundaries of each hole and centroids of them. Finally, the grayscale image was showed and plotted the numbers of magnetic beads chains on the centroids of each of them.

Step 7: The user can select the desired magnetic beads chains. Furthermore, the user gave the information of one magnetic bead size for the quantification of the selected chain. Using prompt function, the first question asked to the user ‘Which accumulations would you like to get information:' and using input function the answer was obtained. The bead size information was obtained via question ‘Please input your bead size in um:’ as well. The picture of plotted magnetic bead chains are shown in Figure 4.1.2 e.

Step 8: The accumulation of magnetic beads length and width were found and using the information of beads size, the number of beads in the selected chain was obtained. For the transformation of the magnetic bead size in pixel, the one bead size on the optical microscope image and cell phone image were measured respectively. Then the information was used as a reference pixel. By dividing the length of the chain to bead pixel size, the numbers of magnetic beads were acquired.

Step 9: The selected accumulation was shown to the user with the information of chain x and y-direction length, area, and magnetic beads number. To show the information, imcrop function was used to crop sub-image from the main image and sprint function was used to print the information, which is shown in Figure 4.1.2 f.

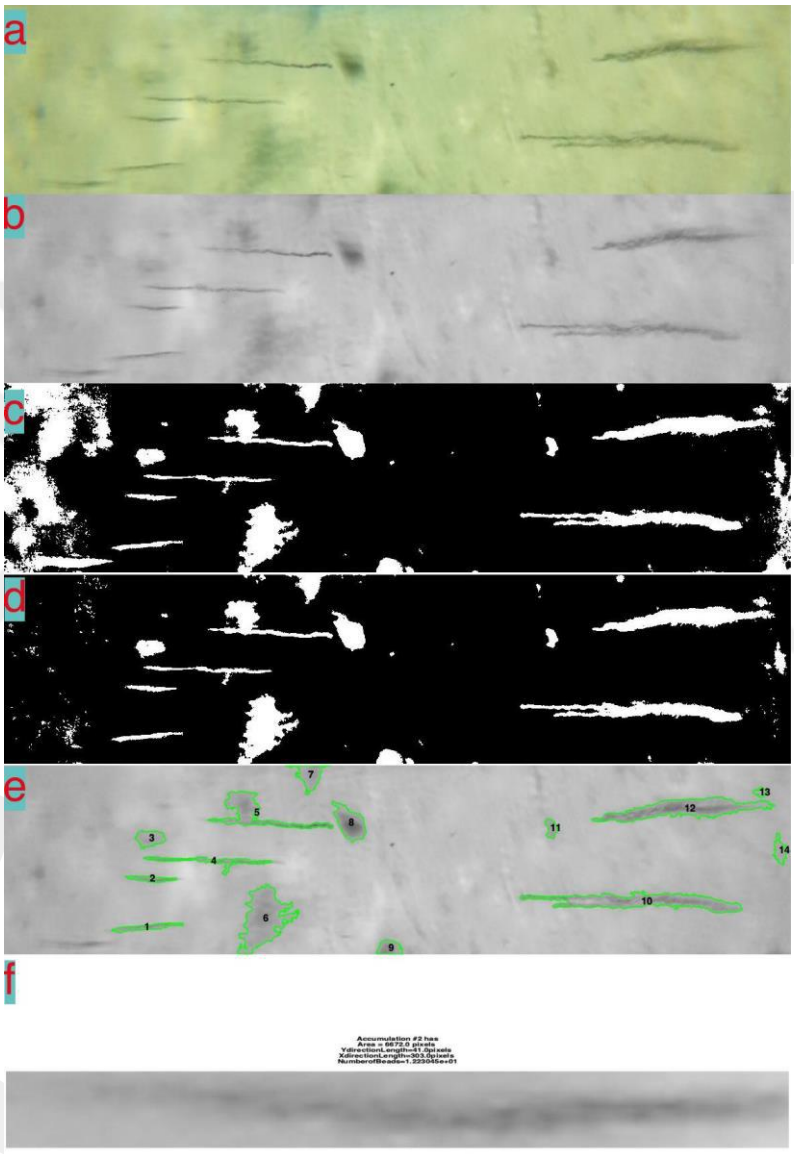

Figure 4.1.2 The image processing method applied to cell phone microscopy images. (a) RGB image used as an input; (b) grayscale image converted from RGB; (c) binary image, obtained using mean and standard deviation method; (d) filtered binary image using morphological operations: imclearborder and bwareaopen; (e) the boundaries of magnetic beads chain and numbers on plotted on original image by filtering background noise to user for the selection of desired chain information; (f) selected chain information, for this example second chain was selected.

4.2 Magnetic Beads Detection on Diffraction Gratings

In this work [2], we provide a new approach for the quantification of immunomagnetic beads on micro-contact printed gratings based on the image processing method. To produce micro-contact printed grating, streptavidin-coated immunomagnetic beads are employed. The brief explanation of creating micro-contact gratings is the PDMS stamp containing 20-μm-line was cleaned and incubated with a BBSA solution. The gold chips were cut and stamped by prepared the PDMS stamp. Then, the gold chips were incubated in the solution of BSA. Finally, the created gold chip containing the BBSA pattern was incubated with different concentrations (0.0335 mg/mL, 0.067 mg/mL, 0.67 mg/mL and 6.7 mg/mL) of streptavidin coated immunomagnetic beads as shown in Figure 4.2.1 In this work, analyzing immunomagnetic beads that were bond on a diffraction grating based on the image processing technique is simple, low-cost and rapid different from previous works such as [114], [109].

The images are recorded from a cell phone microscopy as shown in Figure 4.2.1, then enhanced and analyzed. The image enhancement provides that the cell phone microscopy can be a different option to investigate magnetic beads on micro contact grating. This method can assist to accomplish the limitations of spherical ball lens. In this method, Matlab Image Processing Toolbox (2014b) version is employed on the acquired images by the cell phone microscope, similar work is done in the previous sub-section.

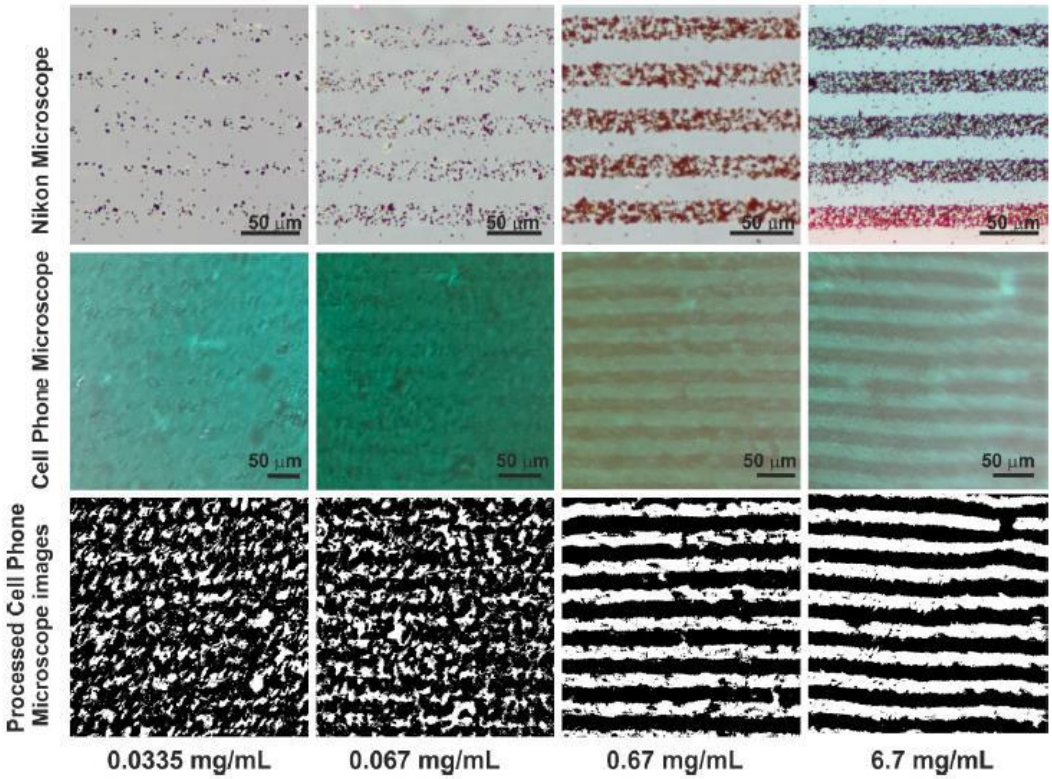

Figure 4.2.1 Images of self-assembled gratings by varying concentrations of immunomagnetic beads on micro-contact printing acquired by cell phone microscope and optical microscope used as a reference microscope. The top row is recorded from the optical microscope (Nikon) and the second row is recorded from the cell phone microscope. The bottom row is processed images acquired by the cell phone microscope.

Figure 4.2.1 illustrates that the images of the gold chips after the immunomagnetic beads self-assembled on the micro contact printed gratings, the coating method is detailed in [2]. Optical micrographs of the certain lines were acquired both the optical microscope and cell phone microscope with 97x magnification. Here, the optical microscope was used as a reference microscope to compare quantifications.

The images recorded from the cell phone microscope were blurry, noisy and they have low quality. Thus, the image-processing algorithm was developed to firstly enhance the images and then to analyze them. The quantification method is explained below.

Step 1: The original image in RGB color space was taken as an input. The input was converted into the grayscale for subsequent processing procedures.

Step 2: The background subtraction was employed to enhance the blurry and noisy background. To provide background subtraction: firstly, the average filter was applied to the grayscale image for removing the shade from the image by smoothing it.

Secondly, the filtered image was opened with strel line having 20 lengths and 180 degrees. Finally, the modified image was subtracted from the grayscale image shown in Figure 4.2.2 C.

Step 4: The image obtained from background subtraction was adjusted to not lose the information of small beads binding on line. The image adjustment was accomplished sum of the adjusted image by adjustment function and dilation of adjusted image. The adjusted image is denoted in Figure 4.2.2 D.

Step 5: The modified image was firstly filled to make a connection between the objects in the image. Then, connected components of each object in the filled image were labeled to gather information of them. Finally, the information of each object was acquired by regional properties function. Boundaries of the objects can be called the detected magnetic beads that were plotted on the image to show them clearly in Figure 4.2.2 E.

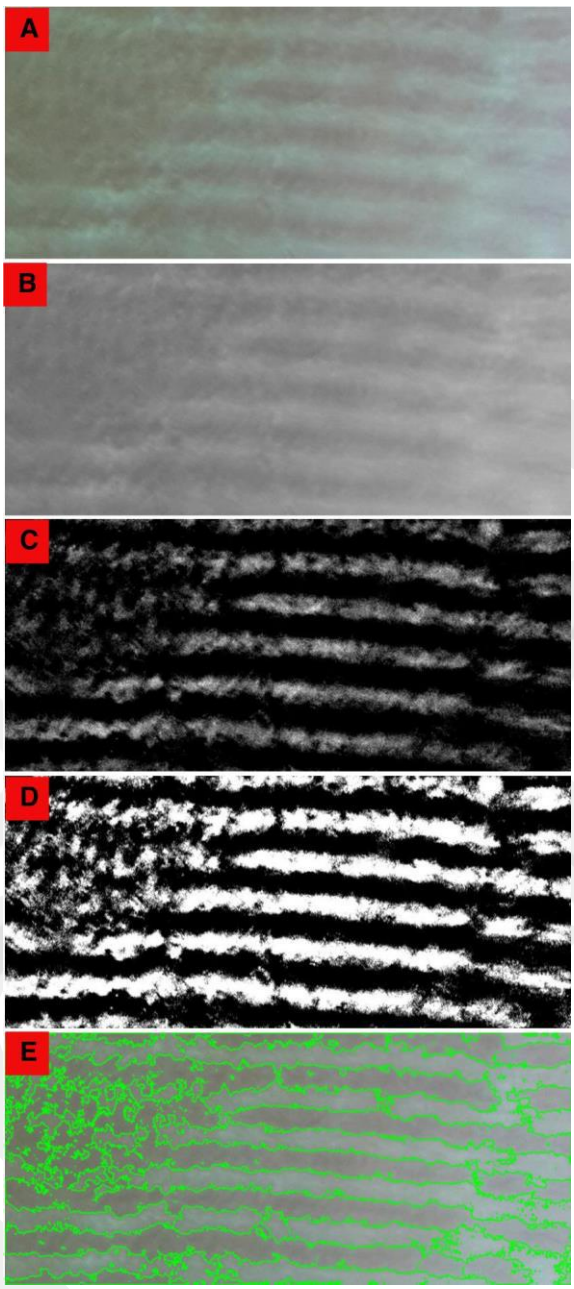

Figure 4.2.2 An example of the result of the image processing method applied to images taken from 0.67 mg/mL solution. (A) original image; (B) gray scale image; (C); background subtracted image; (D) adjusted image; (E) boundaries of magnetic beads plotted on the original image.

4.3 Magnetic Bead and Cell Detection

In this study, we present a method for automatically quantification of immunomagnetic beads and detection of Acute Lymphoblastic Leukemia cells visualized by an optical microscope, which is based on image processing methods. CD34 and CD19 antibodies (magnetic beads) were used to detect ALL cells [5]. In this work, unstained ALL cells were employed different from previous researches given above. The detection of unstained leukemia cells may be more difficult compared to stained cells because their pixel intensity values close the background pixels values.

ALL cells CCRF-SB were purchased from ATCC (Rockville, MD) and these cells cultured for the experiments in Erciyes University Biochemistry Laboratory, CD19 antibody was purchased from Biolegend (San Diego, CA). For image acquisition, Nikon (Melville, NY, USA) optical microscope was used. The cells with antibodies solution smeared on the glass slide, then the images taken from different areas. For the processing of the acquired images, MATLAB Image Processing Toolbox (2014b) was employed. The data acquisition flowchart is shown in Figure 4.3.1.

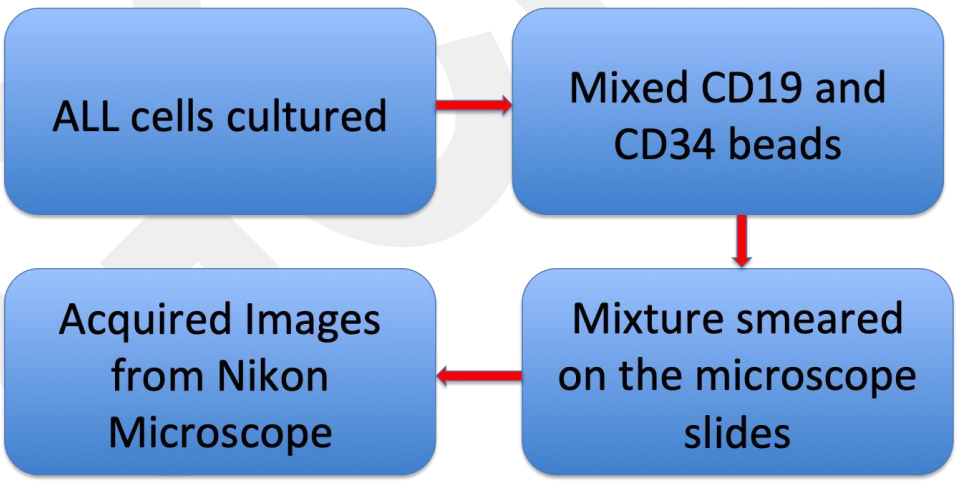

Figure 4.3.1 Illustration of data acquisition for image processing procedure.

CD19 antibodies are used to capture ALL cells by binding them among healthy cells, this binding event provides to label ALL cells and signal amplification of captured cells. Here, the main idea is firstly detection of the magnetic beads and then detection of

ALL cells based on image processing algorithm. The image-processing algorithm provides to gather information about centroids, area, shape, etc. about cells and antibodies. By comparing the centroids of both the cells and the antibodies, the binding antibodies and cells can be quantified. If their centroids are matched or close, it can be an inference that the antibody is bind to the cell.

To develop the image-processing algorithm for detection and quantification of ALL cells, firstly ALL cells binding CD19 antibody images were taken with 100x magnification from microscopic glass slide by optical microscope. Then, an algorithm was developed to segment CD19 magnetic beads and quantify the cells. After that, 20x magnification images were taken from ALL cells without antibody on the microscope slide. The quantification of ALL cells algorithm was developed for the images taken with 20x magnification. Finally, ALL cells binding CD19 antibodies in the images were acquired with 20x magnification. The images taken from optical microscopes with 20x magnification had 8-bit uint in RGB color space and tif format. The processing procedure is explained for 100x magnification, 20x magnification ALL cells and 20x magnification ALL with CD19 antibodies images.

4.3.1 ALL Cells with CD19s in 100x Magnification Images

The method for quantification of the ALL cells can be briefly explained below:

1. Find the CD19 antibodies (magnetic beads),
2. Erode the beads,
3. Find the cells,
4. Compare their regions,
5. Finish the problem.

The provided algorithm of the segmentation process for ALL cells and CD19 antibodies is explained below and the flowchart of the procedure is illustrated in Figure 4.3.1.1.

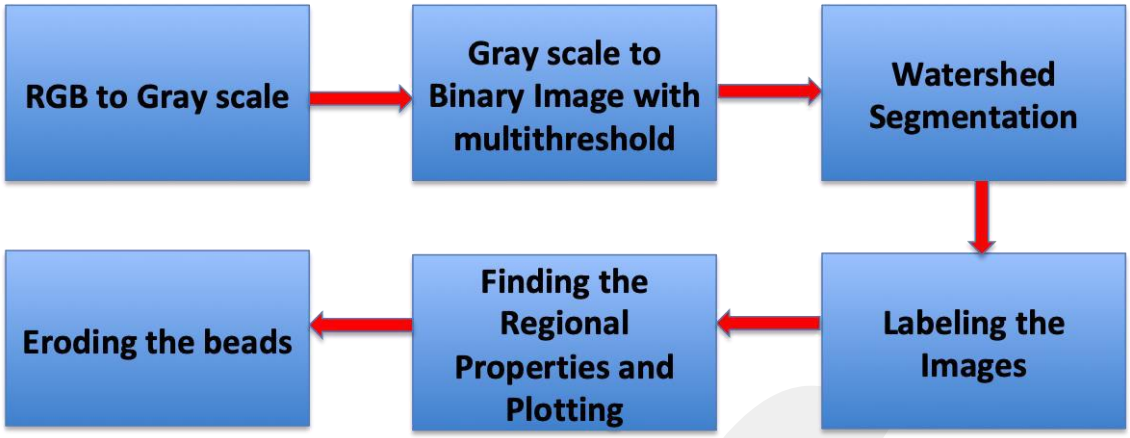

Figure 4.3.1.1 The flowchart of image processing for 100x magnification images.

Step1: RGB image was the input value, which was converted to a grayscale image for subsequent processing procedures. Then, the blue color vector of the gray image was selected for finding the threshold value. Because the blue color vector provided uniform histogram for thresholding.

Step2: The blue color vector in the grayscale image was converted into a binary image by using Otsu's method [117] provided by multithresh function in MathWorks toolbox. Then the holes filled by imfill function.

Step3: The segmentation process was started applying distance transform algorithm on the binary image. The distance transform algorithm was used to calculate the distance of watershed lines for the segmentation of beads before the watershed transform algorithm. Otherwise, the watershed can be failed for over-segmentation. After finding distances, the seed points of beads were found by regional minima function to marker peaks of regions. In Matlab Toolbox, bwdist, imhmin, and watershed functions were used, respectively.

Step 4: Labeling of the objects in the image was performed. Labeling them into RGB color showed the watershed segmentation results.

Step5: The regional properties of each blob were found and plotted the number of them on the beads. To achieve this, regionprops function and plot functions were used.

Step 6: In this step, the beads were eroded. To erode the beads, two approaches were used. The first one is explained here, the second is explained in Step 7.

Firstly, the binary image that was provided by Otsu's threshold was labeled by bwlabel function. Secondly, the information of regions was calculated by regionprops function. Thirdly, the mask was created to erode the beads and it was dilated with strel

disk radius 3. Finally, the mask was applied on the gray scale image using roifill function.

Step 7: In this approach, the binary image was used as a mask. The holes were filled by imfill, and then the resulting image was eroded with strel disk 5 after that applied dilated with strell disk 25. Finally, the modified holes filled by rofill function on the grayscale image.

For solving the main problem, the regional properties of ALL cells required to be found. To develop the algorithm to find out the regions of ALL cells without CD19 in 20x magnification images, the new images were taken and we continued with these images as explained in the subsection below Figure 4.3.1.2.

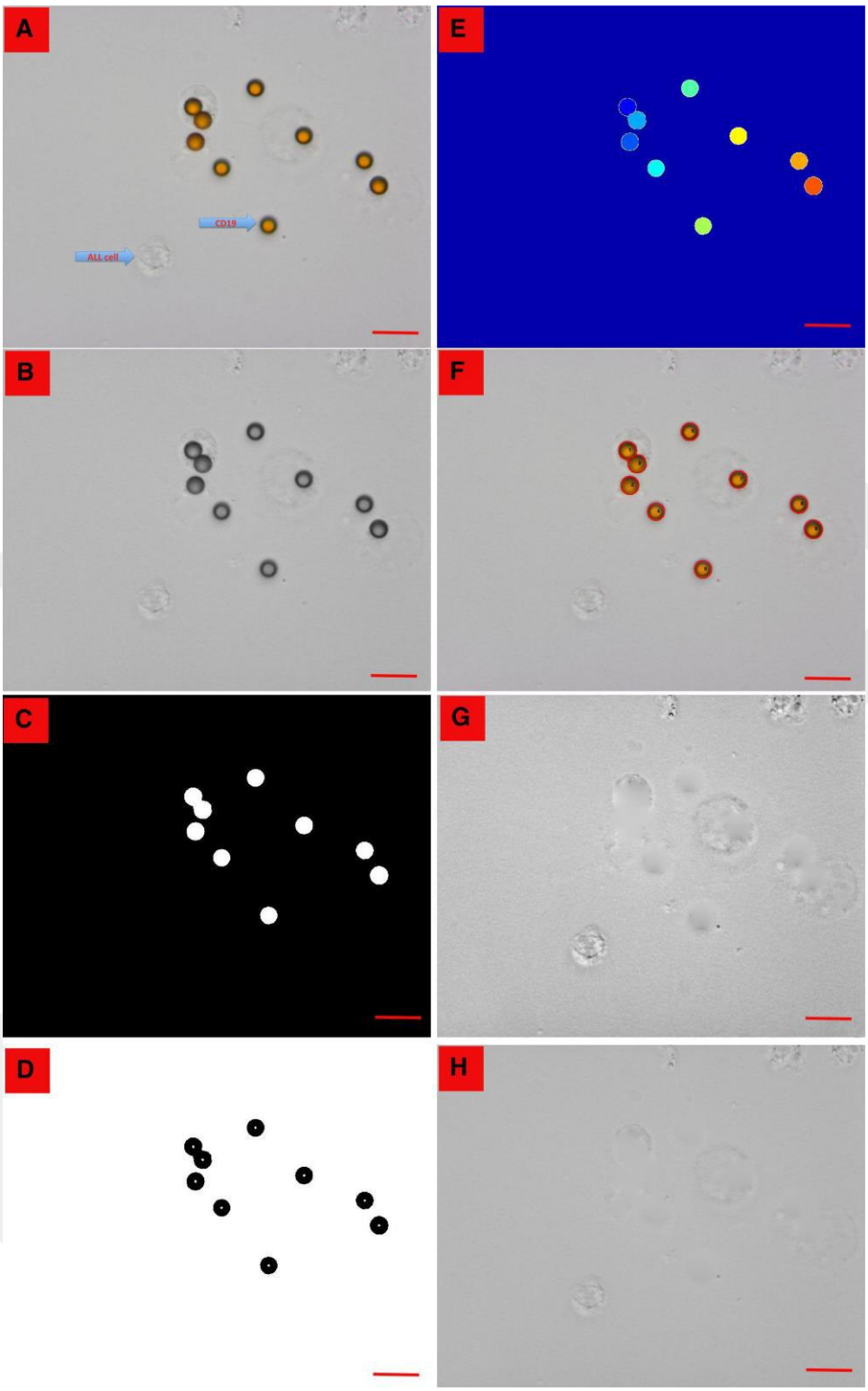

Figure 4.3.1.2 The explanation of the image-processing algorithm. (A) The original image taken from microscope the arrows show the ALL cells and CD19 antibodies; (B) The grayscale image transformed from original image;(C) The binary image converted from the grayscale image using Otsu's multithresholding method;(D) The regional minimums obtained from application of distance transform algorithm and regional minimum functions (E) Applied watershed transform algorithm on (D); (F) Plotting the number of beads segmented via watershed; (G) The first approach of eroding beads using regional properties to create a mask; (H) The second approach of eroding beads applying erosion and dilation on binary image to create a mask. The scale bar is 20 μm for each image.

4.3.2 ALL Cells in 20x Magnification Images

In this section, ALL cells without CD19 antibodies on the images taken from the microscope were segmented and quantified. The flowchart of the image processing procedure is explained in Figure 4.3.2.1. Then, the procedure is explained step by step in the following.

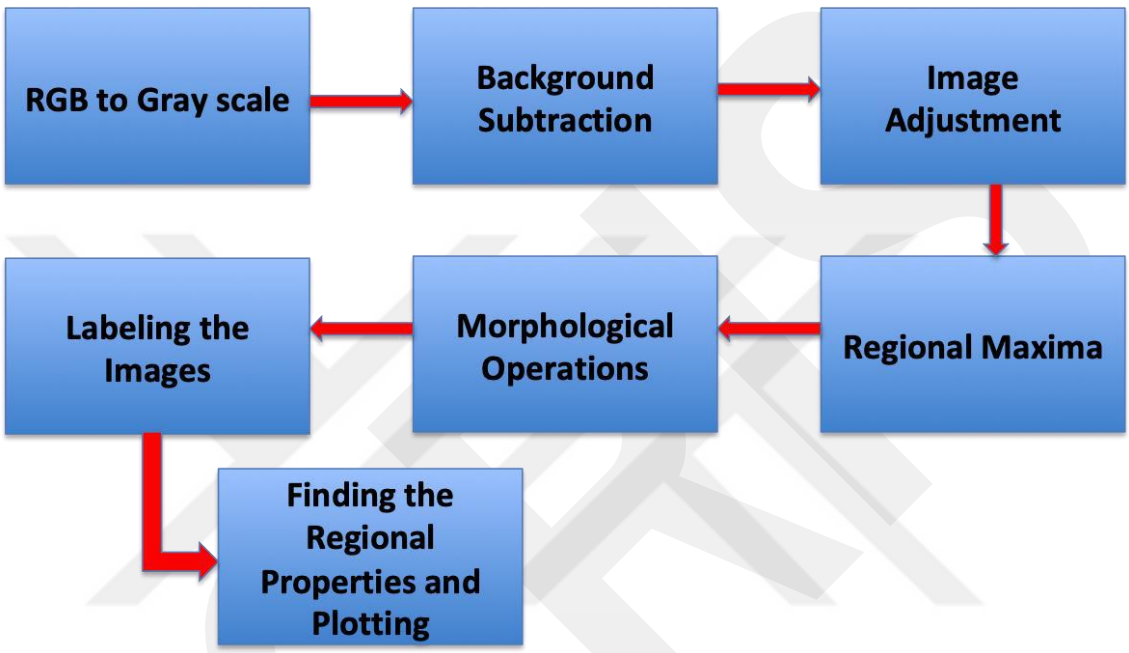

Figure 4.3.2.1 The flowchart of quantification of ALL cells in 20x magnification images.

Step1: RGB was taken as an input and converted into grayscale using the rgb2gray function in Matlab Toolbox. (Figure 4.3.2.2 A and B)

Step 2: In this step, background subtraction was applied to the grayscale image because the intensity values of background and cells were close. Detecting unstained ALL cells in the bright background required to emphasize cells using background subtraction. This procedure also provided to equalize background in close values since the background might have flue area due to the movement of ALL cells' solution.

Firstly, the gray scale image filtered applied average filter with 75 lengths. Then, the resulting image was opened with a strel disk radius 40, which is the radius of a cell. Finally, the modified image was subtracted from the grayscale image. The opened and subtracted images are shown in Figure 4.3.2.2 C and D.

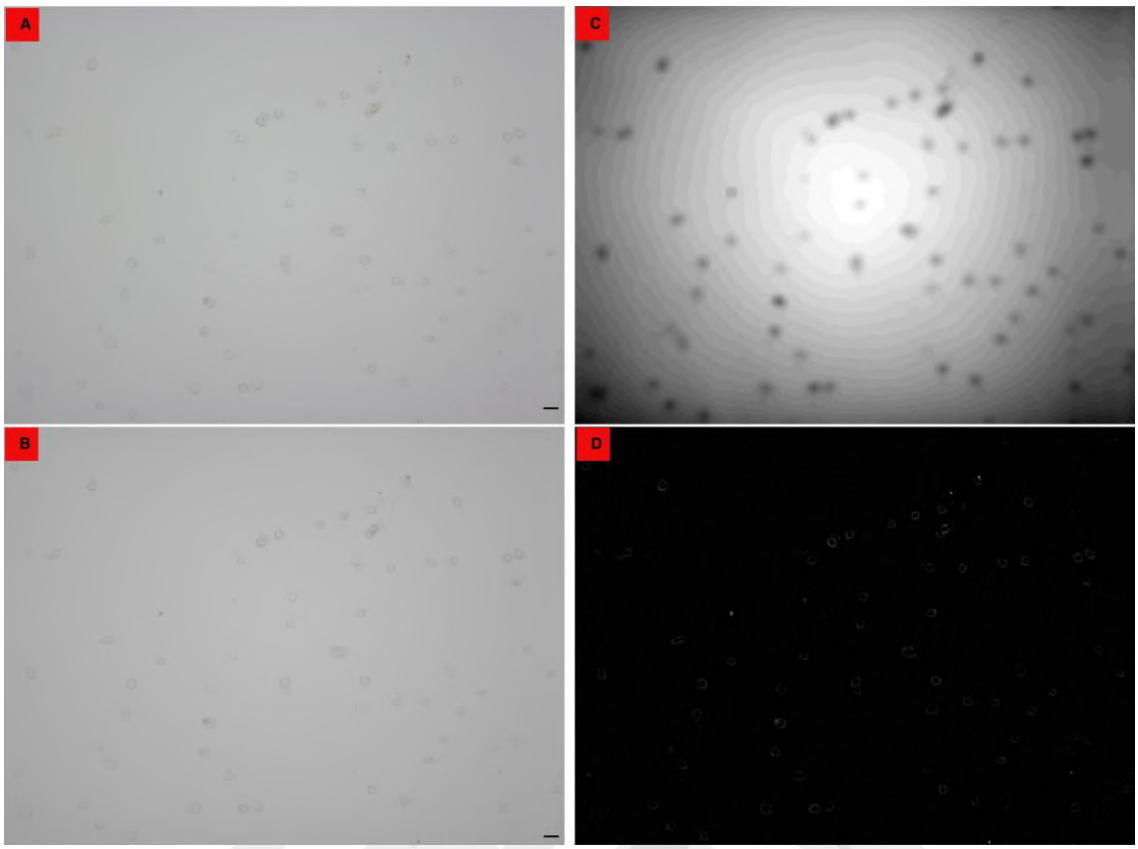

Figure 4.3.2.2 (A) is an original image taken in RGB; (B) is the grayscale image converted from RGB image; (C) is the opened image after applied average filter on the grayscale image shown in B; (D) is the modified image using background subtraction method obtained by subtraction opened image (D) from grayscale (B). The scale bar is 20 μm for each image.

Step 3: The subtracted image was adjusted by intensity adjustment, and then the adjusted image was dilated to emphasize thin objects in the image. The resulting image has obtained the sum of the adjusted and dilated image, as shown in Figure 4.3.2.3 A.

Step 4: The regional maxima were calculated to find out the seed point of the cells, illustrated in Figure 4.3.2.3 B.

Step 5: The morphological operations were used to clean the image and find out the resulting image. Firstly, the opening with the strel radius of 160 cleaned small objects. Then, the holes filled that provided the first shape of cells, filling the connected components. After that, the filled image was eroded and dilated with strel disk radius 10 which cleaned the small filled objects from the image. Finally, reconstructing the modified image segmented the holes, which represent the ALL cells, as shown in Figure 4.3.2.3 C.

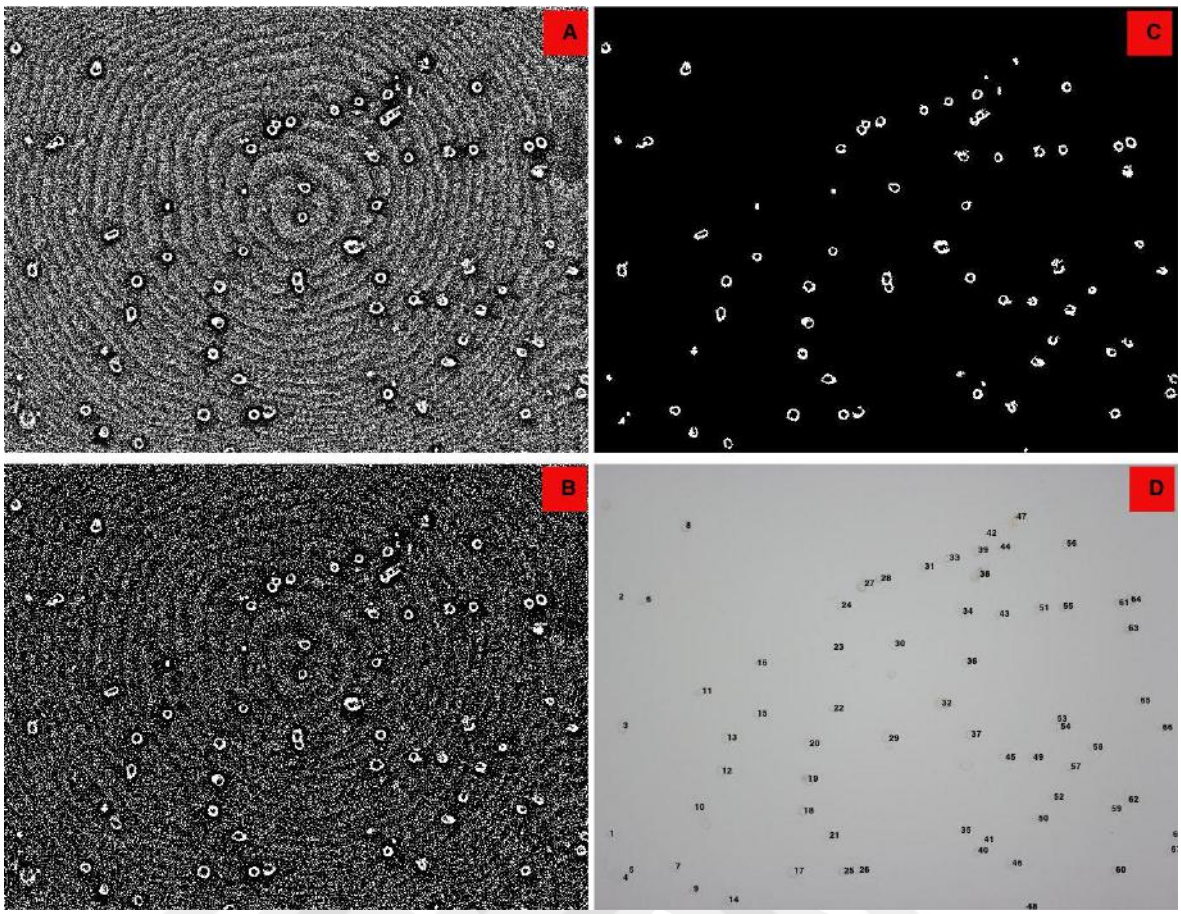

Figure 4.3.2.3 (A) represents the adjusted image obtained by adjustment and dilation; (B) illustrates the regional maxima obtained by A; (C) is the reconstructed image represents the ALL cells; (D) the final image of quantification of ALL cells without CD19 antibodies.

Step 6: The segmented holes were labeled to obtain regional properties of them. Then the regional properties of holes were clarified, thus the ALL cells were quantified. The numbers of ALL cells were plotted on the original image given an input. The resulting image was given in Figure 4.3.2.3 D.

4.3.3 ALL Cells Binding CD19 Antibodies in 20x Magnification Images

In this section, ALL cells binding CD19 antibodies are labeled and provided an algorithm to analyze and quantify them in 20x magnification microscopic images. The flowchart of the provided algorithm is explained in Figure 4.3.3.1.

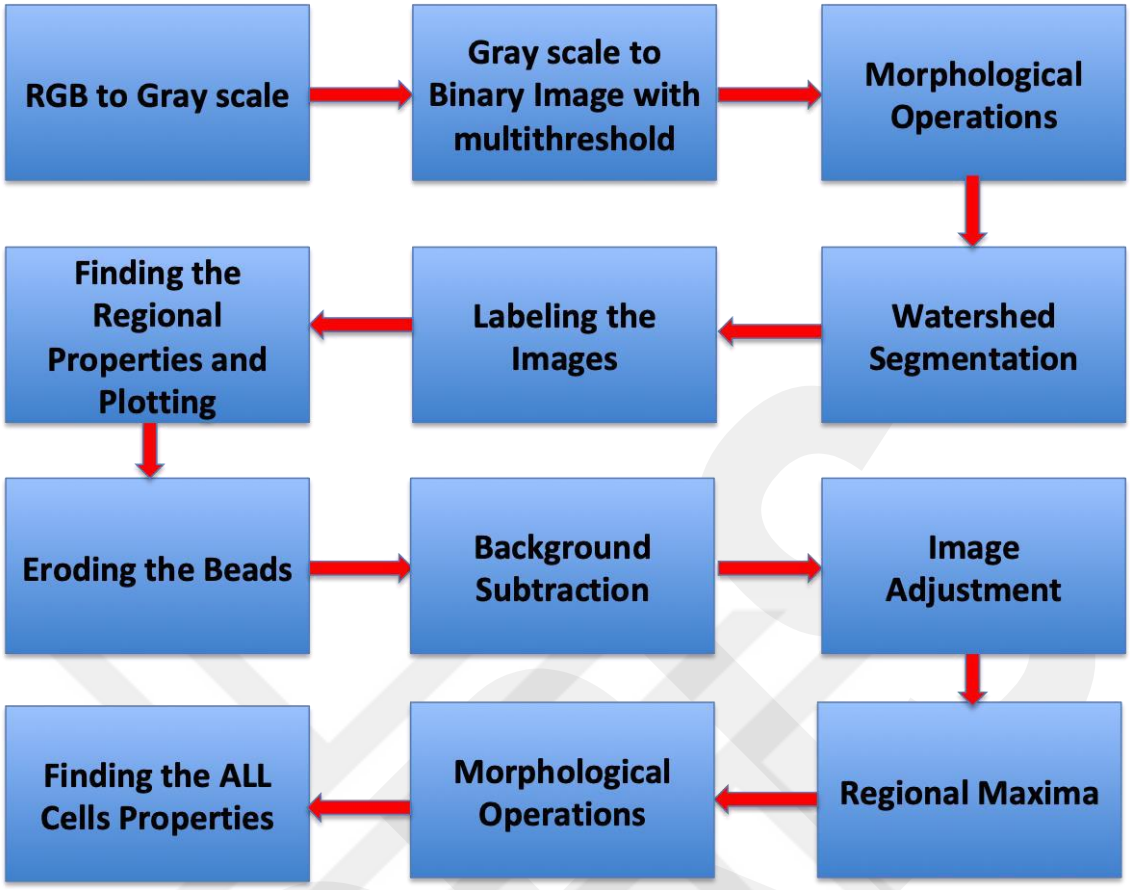

Figure 4.3.3.1 The flowchart of image processing algorithm for the quantification of ALL cells binding CD19 antibodies in 20x magnification images taken from the optical microscope.

In this part of the work, CD19 antibodies/magnetic beads were labeled and quantified for the initial information of image processing. Then, the labeled magnetic beads eroded from the image to acquire the information of ALL cells. Thus, by comparing the center of ALL cells and magnetic beads the meaningful result could be find out.

Quantification of CD19 antibodies

Step 1: As an input, the original image taken from the microscope in RGB color was converted into grayscale to provide better visibility and for further image processing tools.

Step 2: The grayscale image was converted into a binary image using Otsu's thresholding method based on the multithresholding approach (Figure 4.3.3.2 B).

Step 3: Usually, the acquired images from the optical microscope have some variations on the background, which might affect the processing step. Morphological

operations were addressed to overcome these variations and to an applied watershed algorithm. The binary image obtained from the grayscale was filled before morphological operations to prevent over-segmentation. The filled image was opened with strel disk radius 3, which is smaller than beads' radius, thus the additional noise was removed and the desired object was still preserved. The connected objects in the images were separated by eroded with strel disk radius 11, which is about beads size. To obtain bigger bead accumulation as shown in Figure 4.3.3.2 E and F, modified image was reconstructed using the eroded image as a mask and the resulting image was subtracted to obtain small objects like single beads in the image. Considering the beads were obtained close or on the corner of the image that could give incorrect binding information, so they cleared via border clear function.

Step 4: The distance transform algorithm and regional minima methods were employed, respectively to marker the seed point of each object found in the image. Then, the watershed was applied to the image.

Step 5: The segmented image was labeled to obtain regional properties and the information of each segmented object was derived by regional properties algorithm. The segmented objects/beads plotted on the original image as shown in Figure 4.3.3.2 D, E and F.

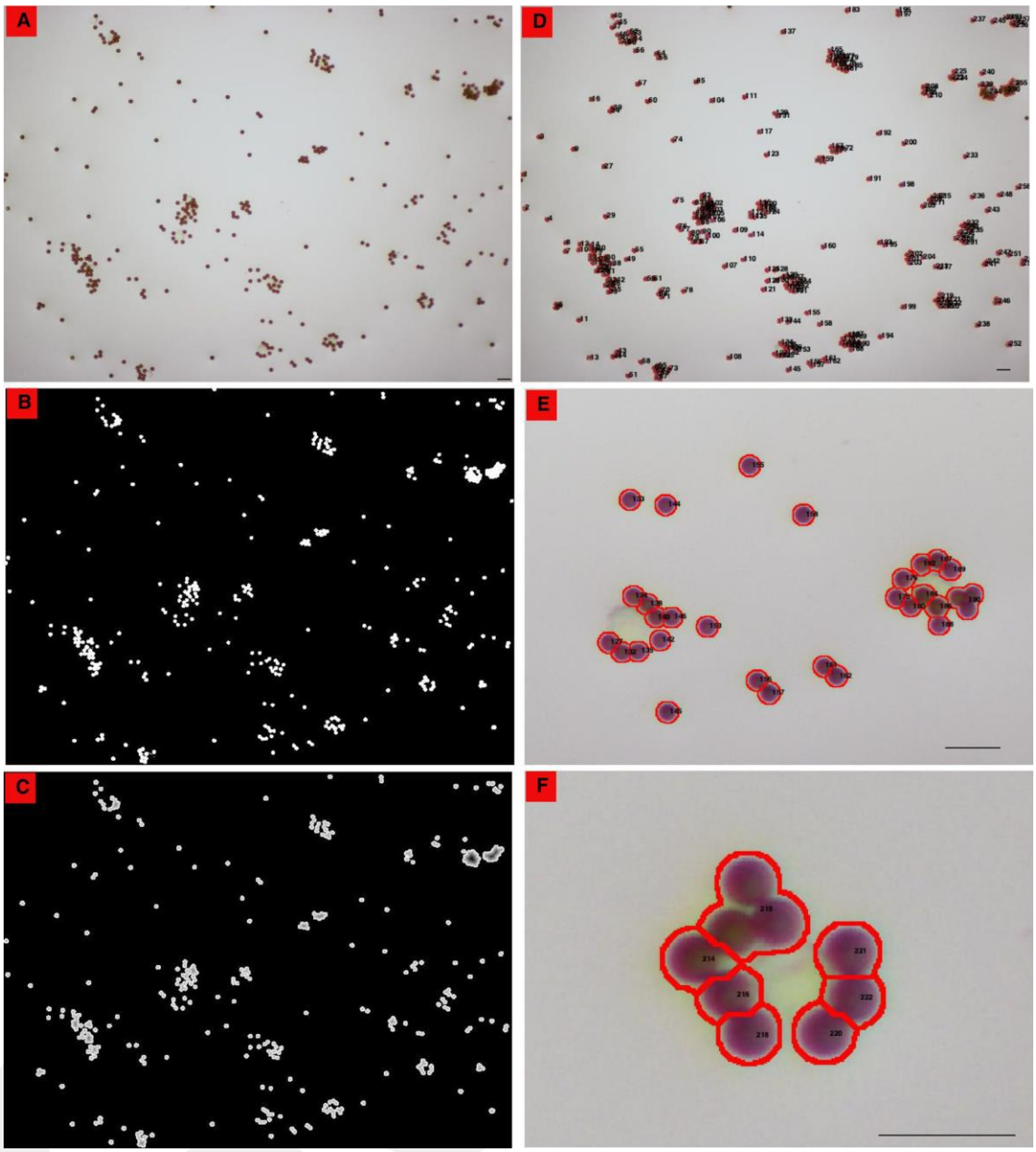

Figure 4.3.3.2 (A) is the original image; (B) is the binary image; (C) illustrates regional minima in the binary image that it is obtained to apply watershed; (D) illustrates the CD19 beads quantification that the segmented beads plotted on the original image; (E) and (F) are cropped images from D to show segmentation better. The scale bar is 20 μm for each image.

Quantification of ALL cells

Here the algorithm was improved to detect ALL cells after eroding CD19 antibodies detected before. The procedure is combination of 4.3.1 and 4.3.2 sub-sections provided upon.

Step 1: For the eroding of magnetic beads from the original image, the mask was created from the binary image that was obtained from the grayscale image via the

multithresholding methods as used before. The binary image was eroded with the strel disk radius 5 and the modified image was dilated with the strel disk radius 30. Implementing obtained mask on the grayscale image filled the objects in the image, thus the beads were cleared from the image. The original image and the images are shown in Figure 4.3.3.3 A. The modified image obtained in the previous step was required to smooth since it had some variations like the flue area on it. Flatting the background was provided to detect cells even they were embedded in the flue area. To succeed, the average filter was initially applied to the image with 75 lengths. Then, the opening with the strel disk 40, which is the radius of one cell, was applied on the smoothed image obtained by the average filter. After that, the areas of the cells were emphasized via subtraction of the opened image from Figure 4.3.3.3 B. The image resulted from subtraction is shown in Figure 4.3.3.3 C.

Step 3: The image acquired via background subtraction was adjusted to open up regional maxima. The adjustment has performed the sum of the adjusted image dilated of the adjusted image. This procedure provided to emphasize the object of gathered from background subtraction. Then, the regional maxima of the image were obtained by applying the regional maxima function. After that, the holes were filled in the image to make a bridge between the objects. Finally, the opening area method was performed to clear small objects from the image (Figure 4.3.3.3 D).

Step 4: The morphological operations were used to find out cells in the image. To perform this, the objects in the obtained image in step 3 were filled to apply the following operations. The object filled image was eroded with the strel disk radius 10 and then dilated with the same strel. The dilated image and the image obtained in step 3 reconstructed to clear small objects from the image. The reconstruction result is shown in Figure 4.3.3.3 E.

Step 5: The objects in the resulting image were labeled and the information of them was found. The detected cells were numbered as illustrated in Figure 4.3.3.3 F, G and H.

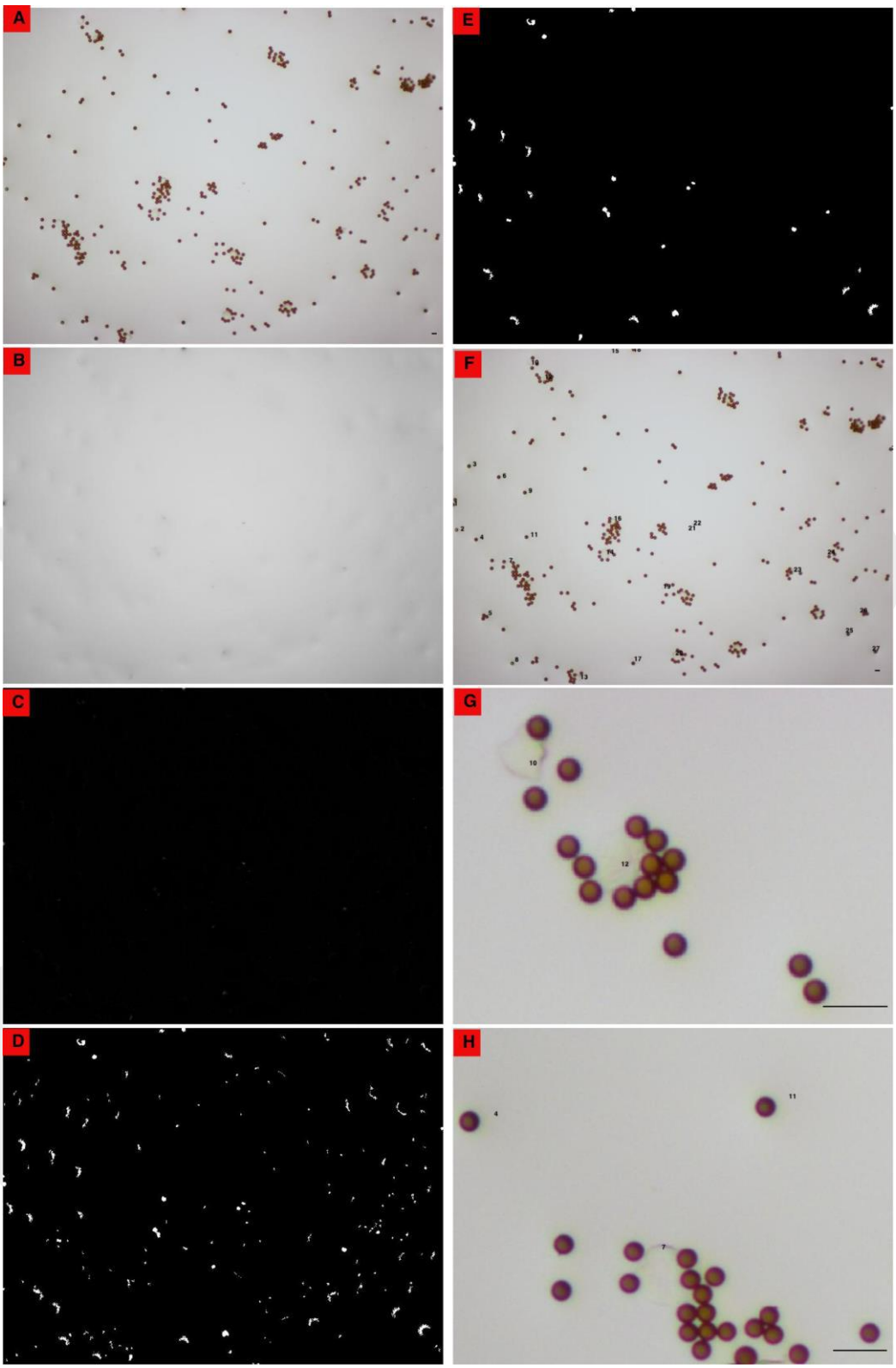

Figure 4.3.3.3 (A) is the original image; (B) is the obtained image after eroding the magnetic beads from original image; (C) The application of background subtraction on B; (D) illustrates the regional maxima after adjusting C and finding maximum field in the image; (E) illustrates the reconstructed images obtained by morphological operations that are used to label the blobs and quantify them; (F) shows the detected ALL cells in the image; (G) and (H) is the part of the resulting image zoomed to show the ALL cells clearly. The scale bar is 20 μm for each image.

Chapter 5

5 Conclusions and Future Prospects

In this thesis, we aimed to perform an automated image processing system for quantification of the magnetic beads and ALL cells taken from cell phone and optical microscopy by employing MATLAB Image Processing Toolbox.

Firstly, the solution of the immunomagnetic beads like ferromagnetic beads and superparamagnetic beads with PBS was prepared and drop on the microscope slide under an applied external 16-mT magnetic field then the accumulation of the beads recorded by cell phone microscopy, which was constructed on spherical ball lens. The acquired images were processed in a cloud server for the quantification of magnetic accumulation and segment each of the beads in the flocculation. The properties of magnetic accumulations such as area, length, etc. and the number of magnetic beads in selected accumulation were gathered.

The automated image processing algorithm for the magnetic beads open up on-site testing utilizing easy operation and portable cell phone microscopy set up. For the future work, the cell phone microscope can be used to detect target molecule such as virus, protein, and cell by binding the immunomagnetic beads. Furthermore, the cell phone application can be created to provide homecare testing for the patients.

Secondly, the image-processing algorithm was developed for the quantification of immunomagnetic beads bound on micro-contact diffraction gratings. For the different concentrations of magnetic beads, solutions were prepared and the images for each concentration were acquired from both the cell phone microscope and the optical microscopy used as a reference microscope. Using the image processing methods the cell phone and the optical microscope images were processed. Then, the pixel areas of magnetic beads were gathered for both microscopy and the results were confronted. The comparison of images for two microscopies showed that the algorithm worked better in optical microscopy images than cell phone microscopy images.

For this work, the future prospect can be to improve the image-processing algorithm for cell phone images. The second aim can be to use a target molecule for

labeling them by using immunomagnetic beads binding features. This method can provide a point of care diagnosis for biosensor applications as well.

Finally, we provide an automated image-processing algorithm for detecting and quantification of ALL cells and CD19 antibodies, which is also called magnetic beads to clarify the impact of chemotherapy. The magnetic beads were used to capture ALL cells by binding them that provide to detect ALL cells by image processing algorithm. We worked on 100x magnification images to quantify magnetic beads and ALL cells. The aim of this study was initially to find the center of magnetic beads, then find the center of cells and finally to compare centers. If the center of the ALL cells and magnetic beads is close to each other, it means that they are bound. The image-processing algorithm was enhanced using 20x magnification images. The automated quantification system can be improved for the segmentation of each magnetic bead in the image to capture each ALL cells in the images for future work.

BIBLIOGRAPHY

[1] "https://www.macmillan.org.uk/information-and-support/myeloma/understanding-cancer/what-is-myeloma.html." .

[2] K. İçöz, "Image Processing and Cell Phone Microscopy to Analyze the Immunomagnetic Beads on Micro-Contact Printed Gratings," *Appl. Sci.*, vol. 6, no. 10, p. 279, 2016.

[3] R. L. Siegel, K. D. Miller, and A. Jemal, "Cancer statistics, 2019.," *CA. Cancer J. Clin.*, 2019.

[4] "Leukemia in children." [Online]. Available: https://www.cancer.org/cancer/leukemia-in-children/detection-diagnosis-staging/how-diagnosed.html.

[5] K. Icoz, M. C. Soylu, Z. Canikara, and E. Unal, "Quartz-crystal Microbalance Measurements of CD19 Antibody Immobilization on Gold Surface and Capturing B Lymphoblast Cells: Effect of Surface Functionalization," *Electroanalysis*, vol. 30, no. 5, pp. 834–841, 2018.

[6] N. Hazwani, A. Halim, M. Y. Mashor, and R. Hassan, "Automatic Blasts Counting for Acute Leukemia Based on Blood," *Int. J. Res. Rev. Comput. Sci.*, vol. 2, no. 4, pp. 971–976, 2011.

[7] Y. Purwar, S. L. Shah, G. Clarke, A. Almugairi, and A. Muehlenbachs, "Automated and unsupervised detection of malarial parasites in microscopic images.," *Malar. J.*, vol. 10, no. 1, p. 364, 2011.

[8] N. E. Ross, C. J. Pritchard, D. M. Rubin, and A. G. Dus??, "Automated image processing method for the diagnosis and classification of malaria on thin blood smears," *Med. Biol. Eng. Comput.*, vol. 44, no. 5, pp. 427–436, 2006.

[9] F. B. Tek, A. G. Dempster, and I. Kale, "Computer vision for microscopy diagnosis of malaria," *Malar. J.*, vol. 8, no. 1, p. 153, 2009.

[10] S. Zafari, T. Eerola, J. Sampo, H. Kälviäinen, and H. Haario, "Segmentation of Overlapping Elliptical Objects in Silhouette Images," *IEEE Trans. Image Process.*, vol. 24, no. 12, pp. 5942–5952, 2015.

[11] C. Park, J. Z. Huang, J. Ji, and Y. Ding, "Segmentation, Inference and Classification of Partially Overlapping Nanoparticles," *IEEE Trans. Pattern Anal. Mach. Intell.*, vol. 35, no. 3, pp. 1–1, 2012.

[12] F. Yi, I. Moon, B. Javidi, D. Boss, and P. Marquetc, "Automated segmentation of multiple red blood cells with digital holographic microscopy," *J. Biomed. Opt.*, vol. 18, no. 2, p. 026006, 2013.

[13] S. Arslan, E. Ozyurek, and C. Gunduz-Demir, "A color and shape based algorithm for segmentation of white blood cells in peripheral blood and bone marrow images," *Cytom. Part A*, vol. 85, no. 6, pp. 480–490, 2014.

[14] N. Malpica *et al.*, "Applying watershed algorithms to the segmentation of clustered nuclei," *Cytometry*, vol. 28, no. 4, pp. 289–297, 1997.

[15] C. F. Koyuncu, E. Akhan, T. Ersahin, R. Cetin-Atalay, and C. Gunduz-Demir, "Iterative H-minima-based marker-controlled watershed for cell nucleus segmentation," *Cytom. Part A*, vol. 89, no. 4, pp. 338–349, 2016.

[16] X. Yang, H. Li, and X. Zhou, "Nuclei segmentation using marker-controlled watershed, tracking using mean-shift, and Kalman filter in time-lapse microscopy," *IEEE Trans. Circuits Syst. I Regul. Pap.*, vol. 53, no. 11, pp. 2405–2414, 2006.

[17] S. Arslan, T. Ersahin, R. Cetin-Atalay, and C. Gunduz-Demir, "Attributed

relational graphs for cell nucleus segmentation in fluorescence microscopy images," *IEEE Trans. Med. Imaging*, vol. 32, no. 6, pp. 1121–1131, 2013.
[18] Y. Wang, Z. Zhang, H. Wang, and S. Bi, "Segmentation of the clustered cells with optimized boundary detection in negative phase contrast images," *PLoS One*, vol. 10, no. 6, 2015.
[19] J. S. Park, M. J. Oh, and S. Han, "Fish disease diagnosis system based on image processing of pathogens' microscopic images," in *Proceedings of the Frontiers in the Convergence of Bioscience and Information Technologies, FBIT 2007*, 2007, pp. 878–883.
[20] M. A. Alyassin *et al.*, "Rapid automated cell quantification on HIV microfluidic devices," *Lab Chip*, vol. 9, no. 23, pp. 3364–3369, 2009.
[21] X. Guo and F. Yu, "A method of automatic cell counting based on microscopic image," *Proc. - 2013 5th Int. Conf. Intell. Human-Machine Syst. Cybern. IHMSC 2013*, vol. 1, pp. 293–296, 2013.
[22] C. Raje and J. Rangole, "Detection of Leukemia in microscopic images using image processing," *2014 Int. Conf. Commun. Signal Process.*, pp. 255–259, 2014.
[23] N. Patel and A. Mishra, "Automated Leukaemia Detection Using Microscopic Images," in *Procedia Computer Science*, 2015, vol. 58, pp. 635–642.
[24] D. K. T. Le, A. A. Bui, Z. Yu, and F. M. Bui, "An automated framework for counting lymphocytes from microscopic images," in *2015 International Conference and Workshop on Computing and Communication, IEMCON 2015*, 2015.
[25] H. Danyali, M. S. Helfroush, and Z. Moshavash, "Robust leukocyte segmentation in blood microscopic images based on intuitionistic fuzzy divergence," *2015 22nd Iran. Conf. Biomed. Eng. ICBME 2015*, no. November, pp. 275–280, 2016.
[26] L. Putzu, G. Caocci, and C. Di Ruberto, "Leucocyte classification for leukaemia detection using image processing techniques," *Artif. Intell. Med.*, vol. 62, no. 3, pp. 179–191, 2014.
[27] S. Malhotra, A. Verma, N. Tyagi, and V. Kumar, "Biosensors : Principle , Types and Applications," *IJARIIE-ISSN J.*, vol. 3, no. 2, pp. 3639–3644, 2017.
[28] C. Karunakaran, R. Rajkumar, and K. Bhargava, "Introduction to Biosensors," *Biosens. Bioelectron.*, no. June, pp. 1–68, 2015.
[29] J. Ali, J. Najeeb, M. Asim Ali, M. Farhan Aslam, and A. Raza, "Biosensors: Their Fundamentals, Designs, Types and Most Recent Impactful Applications: A Review," *J. Biosens. Bioelectron.*, vol. 08, no. 01, pp. 1–9, 2017.
[30] K. İçöz, "Fundamentals of BioMEMS Lecture 4 AGÜ-EEE," no. 1. 2016.
[31] Y. Alapan, K. Icoz, and U. A. Gurkan, "Micro-and nanodevices integrated with biomolecular probes," *Heal. Res. Alliance Memb.*, vol. 33, no. 8, pp. 1727–1743, 2015.
[32] S. K. Metkar and K. Girigoswami, "Diagnostic biosensors in medicine – A review," *Biocatal. Agric. Biotechnol.*, vol. 17, pp. 271–283, 2019.
[33] M. Mascini, "A Brief Story of Biosensor Technology," *Biotechnol. Appl. Photosynth. Proteins Biochips, Biosens. Biodevices*, pp. 4–10, 2006.
[34] W. R. Heineman and W. B. Jensen, "Leland C. Clark Jr. (1918–2005)," *Biosens. Bioelectron.*, vol. 21, no. 8, pp. 1403–1404, 2006.
[35] L. C. Clark and C. Lyons, "Electrode Systems for Continuous Monitoring in Cardiovascular Surgery," *Ann. N. Y. Acad. Sci.*, vol. 102, no. 1, pp. 29–45, 1962.
[36] S. J. UPDIKE and G. P. HICKS, "The Enzyme Electrode," *Nature*, vol. 214, p. 986, Jun. 1967.

[37] G. G. Guilbault and J. G. Montalvo, “Urea-specific enzyme electrode,” *J. Am. Chem. Soc.*, vol. 91, no. 8, pp. 2164–2165, Apr. 1969.
[38] E. H. Yoo and S. Y. Lee, “Glucose biosensors: An overview of use in clinical practice,” *Sensors*, vol. 10, no. 5, pp. 4558–4576, 2010.
[39] J. K. Patra, D. K. Mahato, and P. Kumar, *Biosensor Technology—Advanced Scientific Tools, With Special Reference to Nanobiosensors and Plant- and Food-Based Biosensors*. Elsevier Inc., 2019.
[40] U. Anik, *Electrochemical medical biosensors for POC applications*. Elsevier Ltd, 2016.
[41] C. L. Martin, “i-STAT – Combining Chemistry and Haematology in PoCT,” *Clin. Biochem Rev.*, vol. 31, no. August, pp. 81–84, 2010.
[42] P. Testing, “The i-STAT System : Comprehensive A Wide Range of Cartridges for Diagnostic Testing *,” *Https://Www.Abbottpointofcare.Com/Poc-Work*. [Online]. Available: https://www.abbottpointofcare.com/poc-work.
[43] D. Grieshaber, R. MacKenzie, J. Vörös, and E. Reimhult, “Electrochemical biosensors - Sensor principles and architectures,” *Sensors*. 2008.
[44] J. W. Xueji Zhang,Huangxian Ju, *Xueji Zhang, Huangxian Ju, Joseph Wang-Electrochemical Sensors, Biosensors and their Biomedical Applications (2007).pdf*, vol. 91. 2017.
[45] D. Thevenot *et al.*, “Electrochemical biosensors : recommended definitions and classification To cite this version : HAL Id : hal-01084678 Technical report Electrochemical biosensors : recommended definitions and classification,” *Biosens. Bioelectron.*, vol. 16, pp. 121–131, 2001.
[46] A. Gottschalk, M. Breulmann, E. Fetter, K. Kretschmer, and M. Bastian, “Electrochemical Biosensors - Sensor Principles and Architectures,” *Sensors*, vol. 96, no. 7, pp. 48–50, 2008.
[47] E. Bakker and E. Pretsch, “Potentiometric sensors for trace levels,” *TrAC - Trends Anal. Chem.*, vol. 24, no. 3, pp. 199–207, 2005.
[48] S. M. Borisov and O. S. Wolfbeis, “Borisov2008.Pdf,” no. 941, 2008.
[49] H. Sharma and R. Mutharasan, “Review of biosensors for foodborne pathogens and toxins,” *Sensors Actuators, B Chem.*, vol. 183, pp. 535–549, 2013.
[50] A. Roda and M. Guardigli, “Analytical chemiluminescence and bioluminescence: Latest achievements and new horizons,” *Anal. Bioanal. Chem.*, vol. 402, no. 1, pp. 69–76, 2012.
[51] A. Touhami, “Biosensors and Nanobiosensors: Design and Applications,” 2014.
[52] P. D. Bonnet, “The impact of medicare and other federal health legislation on U. S. Teaching hospitals,” *Acad. Med.*, vol. 42, no. 5, pp. 385–391, 1967.
[53] Mohammed Zourob (eds.), “Recognition Receptors in Biosensors,” in *Recognition Receptors in Biosensors*, 2010, p. 849.
[54] D. W. G. Morrison, M. R. Dokmeci, U. Demirci, and A. Khademhosseini, “Clinical Applications of Micro- and Nanoscale Biosensors,” in *Biomedical Nanostructures*, no. 1, 2007, pp. 439–460.
[55] V. Perumal and U. Hashim, “Advances in biosensors: Principle, architecture and applications,” *J. Appl. Biomed.*, vol. 12, no. 1, pp. 1–15, 2014.
[56] P. J. Conroy, S. Hearty, P. Leonard, and R. J. O’Kennedy, “Antibody production, design and use for biosensor-based applications,” *Semin. Cell Dev. Biol.*, vol. 20, no. 1, pp. 10–26, 2009.
[57] C. I. L. Justino, A. C. Freitas, R. Pereira, A. C. Duarte, and T. A. P. Rocha Santos, “Recent developments in recognition elements for chemical sensors and biosensors,” *TrAC - Trends Anal. Chem.*, vol. 68, pp. 2–17, 2015.

[58] P. D. Skottrup, M. Nicolaisen, and A. F. Justesen, “Towards on-site pathogen detection using antibody-based sensors,” *Biosens. Bioelectron.*, vol. 24, no. 3, pp. 339–348, 2008.
[59] C. L. Chang *et al.*, “Circulating tumor cell detection using a parallel flow micro-aperture chip system,” *Lab Chip*, vol. 15, no. 7, pp. 1677–1688, 2015.
[60] J. Labuda *et al.*, “Electrochemical nucleic acid-based biosensors : Concepts , terms , and methodology (IUPAC Technical Report)*,” vol. 82, no. 5, pp. 1161–1187, 2010.
[61] P. L. Q. Wang, *Cell-based biosensors: principles and applications*. 2009.
[62] V. A. T. A. Q. H. D. K. S. P. J. Hornsby, “Tissue-Based Biosensors,” in *Recognition Receptors in Biosensors*, Mohammed Zourob (eds.), Ed. New Yor,NY: Springer, 2010, pp. 365–381.
[63] Q. Liu, N. Hu, F. Zhang, H. Wang, W. Ye, and P. Wang, “Neurosecretory cell-based biosensor: Monitoring secretion of adrenal chromaffin cells by local extracellular acidification using light-addressable potentiometric sensor,” *Biosens. Bioelectron.*, vol. 35, no. 1, pp. 421–424, 2012.
[64] E. Torres-Chavolla and E. C. Alocilja, “Aptasensors for detection of microbial and viral pathogens,” *Biosensors and Bioelectronics*, vol. 24, no. 11. pp. 3175–3182, 2009.
[65] Y. X. Wang, Z. Z. Ye, C. Y. Si, and Y. Bin Ying, “Application of aptamer based biosensors for detection of pathogenic microorganisms,” *Fenxi Huaxue/ Chinese Journal of Analytical Chemistry*, vol. 40, no. 4. Changchun Institute of Applied Chemistry, Chinese Academy of Sciences, pp. 634–642, 2012.
[66] B. Strehlitz, N. Nikolaus, and R. Stoltenburg, “Protein detection with aptamer biosensors,” *Sensors*, vol. 8, no. 7. pp. 4296–4307, 2008.
[67] E. B. Bahadir and M. K. Sezgintürk, “Applications of commercial biosensors in clinical, food, environmental, and biothreat/biowarfare analyses,” *Anal. Biochem.*, vol. 478, no. March, pp. 107–120, 2015.
[68] J. H. T. Luong, K. B. Male, and J. D. Glennon, “Biosensor technology: Technology push versus market pull,” *Biotechnology Advances*, vol. 26, no. 5. pp. 492–500, 2008.
[69] WHO, *Global Health Risks*. 2009.
[70] WHO and World Health Organisation, “WHO | Diabetes,” *World Health Organization (WHO)*, 2017. .
[71] E. B. Bahadir and M. K. Sezgintürk, “Electrochemical biosensors for hormone analyses,” *Biosens. Bioelectron.*, vol. 68, pp. 62–71, 2015.
[72] L. Bueno, W. R. de Araujo, and T. R. L. C. Paixão, *Point of care (POC) medical biosensors for cancer detection*. Elsevier Ltd, 2016.
[73] K. Baryeh, S. Takalkar, M. Lund, and G. Liu, *Introduction to medical biosensors for point of care applications*. Elsevier Ltd, 2016.
[74] S. H. A. Hassan, S. W. Van Ginkel, M. A. M. Hussein, R. Abskharon, and S. E. Oh, “Toxicity assessment using different bioassays and microbial biosensors,” *Environment International*, vol. 92–93. Elsevier Ltd, pp. 106–118, 2016.
[75] R. Gao *et al.*, “Fast and sensitive detection of an anthrax biomarker using SERS-based solenoid microfluidic sensor,” *Biosens. Bioelectron.*, vol. 72, pp. 230–236, 2015.
[76] J. Dubuisson, A. Fehlmann, and P. Petignat, “Management of presumed benign giant ovarian cysts: A minimally invasive technique using the alexis laparoscopic system,” *J. Minim. Invasive Gynecol.*, vol. 22, no. 4, p. 540, 2015.
[77] M. Faraji, Y. Yamini, and M. Rezaee, “magnetic nanoparticles : synthesis ,

stabilization , functionalization , characterization , and applications," *J. Iran. Chem. Soc.*, vol. 7, no. 1, pp. 1–37, 2010.
[78] Q. A. Pankhurst, J. Connolly, S. K. Jones, and J. Dobson, "Applications of magnetic nanoparticles in biomedicine," *J. Phys. D Appl. Phys*, vol. 36, no. 03, pp. 167–181, 2003.
[79] Y. T. Chen, A. G. Kolhatkar, O. Zenasni, S. Xu, and T. R. Lee, *Biosensing using magnetic particle detection techniques*, vol. 17, no. 2300. 2017.
[80] T. Jamshaid *et al.*, "Magnetic particles: From preparation to lab-on-a-chip, biosensors, microsystems and microfluidics applications," *TrAC - Trends Anal. Chem.*, vol. 79, pp. 344–362, 2016.
[81] L. Mohammed, H. G. Gomaa, D. Ragab, and J. Zhu, "Magnetic nanoparticles for environmental and biomedical applications: A review," *Particuology*, vol. 30, pp. 1–14, 2017.
[82] R. S. M. Rikken, R. J. M. Nolte, J. C. Maan, J. C. M. Van Hest, D. A. Wilson, and P. C. M. Christianen, "Manipulation of micro- and nanostructure motion with magnetic fields," *Soft Matter*, vol. 10, no. 9, pp. 1295–1308, 2014.
[83] G. P. Hatch and R. E. Stelter, "Magnetic design considerations for devices and particles used for biological high-gradient magnetic separation (HGMS) systems," *J. Magn. Magn. Mater.*, vol. 225, no. 1–2, pp. 262–276, 2001.
[84] L. Hajba and A. Guttman, "The use of magnetic nanoparticles in cancer theranostics: Toward handheld diagnostic devices," *Biotechnol. Adv.*, vol. 34, no. 4, pp. 354–361, 2016.
[85] J. Chomoucka, J. Drbohlavova, D. Huska, V. Adam, R. Kizek, and J. Hubalek, "Magnetic nanoparticles and targeted drug delivering," *Pharmacol. Res.*, vol. 62, no. 2, pp. 144–149, 2010.
[86] C. Binns, "Medical applications of magnetic nanoparticles," *Front. Nanosci.*, vol. 6, pp. 217–258, 2014.
[87] A. H. Lu, E. L. Salabas, and F. Schüth, "Magnetic nanoparticles: Synthesis, protection, functionalization, and application," *Angew. Chemie - Int. Ed.*, vol. 46, no. 8, pp. 1222–1244, 2007.
[88] J.-G. Zhu, Y. Zheng, and G. A. Prinz, "Ultrahigh density vertical magnetoresistive random access memory (invited)," *J. Appl. Phys.*, vol. 87, no. 9, pp. 6668–6673, 2002.
[89] G. Li *et al.*, "Detection of single micron-sized magnetic bead and magnetic nanoparticles using spin valve sensors for biological applications," in *Journal of Applied Physics*, 2003, vol. 93, no. 10 2, pp. 7557–7559.
[90] W. Shen *et al.*, "Detection of DNA labeled with magnetic nanoparticles using MgO-based magnetic tunnel junction sensors," *J. Appl. Phys.*, 2008.
[91] S. G. Grancharov *et al.*, "Bio-functionalization of monodisperse magnetic nanoparticles and their use as biomolecular labels in a magnetic tunnel junction based sensor," *J. Phys. Chem. B*, vol. 109, no. 26, pp. 13030–13035, 2005.
[92] S. B. Chan *et al.*, "Liver cancer immunoassay with magnetic nanoparticles and MgO-based magnetic tunnel junction sensors," *J. Appl. Phys.*, vol. 111, no. 7, p. 07E505, 2012.
[93] A. Cousins *et al.*, "Novel handheld magnetometer probe based on magnetic tunnelling junction sensors for intraoperative sentinel lymph node identification," *Sci. Rep.*, vol. 5, 2015.
[94] C. D. Damsgaard, B. T. Dalslet, S. C. Freitas, P. P. Freitas, and M. F. Hansen, "Temperature effects in exchange-biased planar hall sensors for bioapplications," *Sensors Actuators, A Phys.*, vol. 156, no. 1, pp. 103–108, 2009.

[95] R. Weissleder *et al.*, “Magnetic sensing technology for molecular analyses,” *Lab Chip*, vol. 14, no. 14, p. 2385, 2014.
[96] R. Qiao, C. Yang, and M. Gao, “Superparamagnetic iron oxide nanoparticles: from preparations to in vivo MRI applications,” *J. Mater. Chem.*, vol. 19, no. 35, pp. 6274–6293, 2009.
[97] N. A. Frey, S. Peng, K. Cheng, and S. Sun, “Magnetic nanoparticles: Synthesis, functionalization, and applications in bioimaging and magnetic energy storage,” *Chemical Society Reviews*, vol. 38, no. 9. pp. 2532–2542, 2009.
[98] J. M. Perez, L. Josephson, T. O’Loughlin, D. Högemann, and R. Weissleder, “Magnetic relaxation switches capable of sensing molecular interactions,” *Nat. Biotechnol.*, vol. 20, no. 8, pp. 816–820, 2002.
[99] S. S. Zalesskiy, E. Danieli, B. Blümich, and V. P. Ananikov, “Miniaturization of NMR Systems: Desktop Spectrometers, Microcoil Spectroscopy, and ‘NMR on a Chip’ for Chemistry, Biochemistry, and Industry,” *Chem. Rev.*, vol. 114, no. 11, pp. 5641–5694, 2014.
[100] D. Eberbeck *et al.*, “Specific binding of magnetic nanoparticle probes to platelets in whole blood detected by magnetorelaxometry,” *J. Magn. Magn. Mater.*, vol. 321, no. 10, pp. 1617–1620, 2009.
[101] S. Ge, X. Shi, J. R. Baker, M. M. Banaszak Holl, and B. G. Orr, “Development of a remanence measurement-based SQUID system with in-depth resolution for nanoparticle imaging,” *Phys. Med. Biol.*, vol. 54, no. 10, pp. 177–188, 2009.
[102] G. G. Kenning *et al.*, “Detection of magnetically enhanced cancer tumors using SQUID magnetometry: A feasibility study,” *Rev. Sci. Instrum.*, vol. 76, no. 1, 2005.
[103] D. Maser *et al.*, “Note: Detection of a single cobalt microparticle with a microfabricated atomic magnetometer,” *Rev. Sci. Instrum.*, vol. 82, no. 8, 2011.
[104] F. Su, C. Xu, M. Taya, K. Murayama, Y. Shinohara, and S. I. Nishimura, “Detection of carcinoembryonic antigens using a surface plasmon resonance biosensor,” *Sensors*, 2008.
[105] F. Ludwig, E. Heim, D. Eberbeck, K. Schwarz, L. Trahms, and M. Schilling, “Comparison and calibration of fluxgate and squid magnetorelaxometry techniques for the characterization of magnetic core-shell nanoparticles,” in *IEEE Transactions on Magnetics*, 2009, vol. 45, no. 10, pp. 4857–4860.
[106] C. B. Kim, E. G. Lim, S. W. Shin, H. J. Krause, and H. Hong, “Magnetic immunoassay platform based on the planar frequency mixing magnetic technique,” *Biosens. Bioelectron.*, vol. 83, pp. 293–299, 2016.
[107] H. Ju, “Signal Amplification for Highly Sensitive Bioanalysis Based on Biosensors or Biochips,” *J. Biochips Tissue Chips*, vol. 02, no. 02, pp. 2–3, 2013.
[108] C. Feng and X. Zhu, “Signal Amplification,” in *Nano-Inspired Biosensors for Protein Assay with Clinical Applications*, Elsevier Inc., 2018, pp. 287–312.
[109] J. Lee, K. Icoz, A. Roberts, A. D. Ellington, and C. A. Savran, “Diffractometric Detection of Proteins using Microbead-based Rolling Circle Amplification,” *NIH Public Access*, vol. 82, no. 197, pp. 3831–3840, 2010.
[110] J. Lei and H. Ju, “Signal amplification using functional nanomaterials for biosensing,” *Chem. Soc. Rev.*, vol. 41, no. 6, pp. 2122–2134, 2012.
[111] K. Mzava, Omary, Tas, Zehra, Icoz, “Magnetic micro / nanoparticle flocculation-based signal amplification for biosensing,” *Int. J. Nanomedicine*, vol. Volume 201, pp. 2619–2631, 2016.
[112] O. Mzava, “Improving Sensitivity of Biosensors By Using Micro / Nano Magnetic Particles,” 2016.

[113] C. L. Chang, Z. Ding, V. N. L. R. Patchigolla, B. Ziaie, and C. A. Savran, "Reflective diffraction gratings from hydrogels as biochemical sensors," *IEEE Sens. J.*, vol. 12, no. 7, pp. 2374–2379, 2012.
[114] G. Acharya, C. L. Chang, D. P. Holland, D. H. Thompson, and C. A. Savran, "Rapid detection of S-adenosyl homocysteine using self-assembled optical diffraction gratings," *Angew. Chemie - Int. Ed.*, vol. 47, no. 6, pp. 1051–1053, 2008.
[115] S. Uchida, "Image processing and recognition for biological images," *Dev. Growth Differ.*, vol. 55, no. 4, pp. 523–549, 2013.
[116] R. Gonzalez, R. , Woods, *Digital Image Processing Gonzalez.pdf*. 2002.
[117] N. Otsu, "A threshold selection method from gray-level histograms," *IEEE Trans. Syst. Man. Cybern.*, vol. 9, no. 1, pp. 62–66, 1979.
[118] L. P. Saxena, "Niblack's binarization method and its modifications to real-time applications: a review," *Artificial Intelligence Review*, 2017.
[119] C. Solomon and T. Breckon, *Fundamentals of Digital Image Processing: A Practical Approach with Examples in Matlab*. 2011.
[120] "https://www.mathworks.com/help/images/ref/imfill.html?searchHighlight=imfill&s_tid=doc_srchtitle." .
[121] R. Gonzalez, R. , Woods, *Digital Image Processing_Gonzalez.pdf*. 2002.
[122] F. Meyer, "Topographic distance and watershed lines," *Signal Processing*, vol. 38, no. 1, pp. 113–125, 1994.
[123] "https://www.mathworks.com/help/images/marker-controlled-watershed-segmentation.html." .
[124] A. Feizi *et al.*, "Wide-field computational imaging of pathology slides using lens-free on-chip microscopy," *Sci. Transl. Med.*, vol. 6, no. 267, pp. 267ra175-267ra175, 2014.
[125] D. N. Breslauer, R. N. Maamari, N. A. Switz, W. A. Lam, and D. A. Fletcher, "Mobile phone based clinical microscopy for global health applications," *PLoS One*, vol. 4, no. 7, pp. 1–7, 2009.
[126] "https://www.microscope.healthcare.nikon.com/products/upright-microscopes/eclipse-ni-u." .
[127] "https://www.apple.com/tr/iphone/." .
[128] J. C. Contreras-Naranjo, Q. Wei, and A. Ozcan, "Mobile Phone-Based Microscopy, Sensing, and Diagnostics," *IEEE J. Sel. Top. Quantum Electron.*, vol. 22, no. 3, 2016.
[129] M. Boussinesq *et al.*, "Point-of-care quantification of blood-borne filarial parasites with a mobile phone microscope," *Sci. Transl. Med.*, vol. 7, no. 286, pp. 286re4-286re4, 2015.
[130] A. Ozcan, "Mobile phones democratize and cultivate next-generation imaging, diagnostics and measurement tools," *Lab Chip*, 2014.
[131] C. Dallet, S. Kareem, and I. Kale, "Real time blood image processing application for malaria diagnosis using mobile phones," *Proc. - IEEE Int. Symp. Circuits Syst.*, pp. 2405–2408, 2014.
[132] N. A. Switz, M. V. D'Ambrosio, and D. A. Fletcher, "Low-cost mobile phone microscopy with a reversed mobile phone camera lens," *PLoS One*, vol. 9, no. 5, 2014.
[133] Z. J. Smith *et al.*, "Cell-phone-based platform for biomedical device development and education applications," *PLoS One*, vol. 6, no. 3, 2011.
[134] I. I. Bogoch *et al.*, "Short report: Mobile phone microscopy for the diagnosis of

soil-transmitted helminth infections: A proof-of-concept study," *Am. J. Trop. Med. Hyg.*, vol. 88, no. 4, pp. 626–629, 2013.
[135] H. C. Koydemir *et al.*, "Rapid imaging, detection and quantification of Giardia lamblia cysts using mobile-phone based fluorescent microscopy and machine learning," *Lab Chip*, vol. 15, no. 5, pp. 1284–1293, 2015.
[136] D. Tseng *et al.*, "Lensfree microscopy on a cellphone," *Lab Chip*, vol. 10, no. 14, pp. 1787–1792, 2010.
[137] S. A. Lee and C. Yang, "A smartphone-based chip-scale microscope using ambient illumination," *Lab Chip*, vol. 14, no. 16, pp. 3056–3063, 2014.
[138] J. S. Cybulski, J. Clements, and M. Prakash, "Foldscope: Origami-based paper microscope," *PLoS One*, vol. 9, no. 6, 2014.
[139] O. Mzava, Z. Taş, V. C. Lafcı, M. A. Çakar, İ. Özdür, and K. İçöz, "Magnetic-particle Based Signal Amplification Method Integrated with Mobile-devices for Low Cost Biosensing," in *Procedia Technology*, 2017, vol. 27, pp. 14–15.